Copyright Warning & Restrictions

The copyright law of the United States (Title 17, United States Code) governs the making of photocopies or other reproductions of copyrighted material.

Under certain conditions specified in the law, libraries and archives are authorized to furnish a photocopy or other reproduction. One of these specified conditions is that the photocopy or reproduction is not to be "used for any purpose other than private study, scholarship, or research." If a, user makes a request for, or later uses, a photocopy or reproduction for purposes in excess of "fair use" that user may be liable for copyright infringement,

This institution reserves the right to refuse to accept a copying order if, in its judgment, fulfillment of the order would involve violation of copyright law.

Please Note: The author retains the copyright while the New Jersey Institute of Technology reserves the right to distribute this thesis or dissertation

Printing note: If you do not wish to print this page, then select "Pages from: first page # to: last page #" on the print dialog screen

ABSTRACT

The Acoustic Properties of Human Femoral Bone

by

Mark Lacianca

Over the last decade, interest has grown in the use of the scanning acoustic microscope (SAM), with a single lens being used for both transmitting and receiving the acoustic signal. A major objective of this thesis was to determine if the transmission and ultrasonic techniques yield similar "quantitative" results, when measuring the elastic constants of human femoral bone. The transmission technique has been used since 1970 to yield values for the elastic properties of calcified tissue. Previously the SAM has been used as a qualitative tool, where an acoustic impedance map is produced. This map can show areas of bone remodelling and resorption at a microscopic level. Therefore, by proving that the SAM can give elastic constant data that corresponds to the values obtained from the transmission technique, a bone section can be directly scanned to give both quantitative and qualitative information.

An experiment was conducted to obtain the acoustic impedance of "individual quadrants" from a human femur section by using the SAM. The acoustic impedance of bone was determined by calibrating the microscope with glass and plexiglass, two materials whose acoustic impedance has been widely documented. These results were compared to the stiffness results measured from the transmission technique, which has two transducers (one is a transmitter, and the other is a receiver). Finally, by retrieving accurate acoustic impedance maps from embedded specimens, there is great promise in the future for assuring the material properties of histological specimens embedded in polymethylmethacrylate.

THE ACOUSTIC PROPERTIES OF HUMAN FEMORAL BONE

by
Mark Lacianca

A Thesis
Submitted to the Faculty of
New Jersey Institute of Technology
in Partial Fulfillment of the Requirements for the Degree of
Master of Science in Biomedical Engineering
October, 1992

APPROVAL PAGE

The Acoustic Properties of Human Femoral Bone

by

Mark Lacianca

Clarence W. Mayott, Ph.D., Thesis Adviser
Assistant Professor of Mechanical Engineering, New Jersey Institute of Technology

---

Mark C. Zimmerman, Ph.D., Committee Member
Assistant Professor of Orthopaedics, UMD-New Jersey Medical School and Adjunct Assistant Professor of Biomedical Engineering, New Jersey Institute of Technology

---

J. Russell Parsons, Ph.D., Committee Member
Associate Professor of Orthopaedics UMD-New Jersey Medical School and Adjunct Associate Professor of Biomedical Engineering, New Jersey Institute of Technology

BIOGRAPHICAL SKETCH

Author: Mark Lacianca

Degree: Master of Science in Biomedical Engineering

Date: October, 1992

Undergraduate and Graduate Education:

- Master of Science in Biomedical Engineering, New Jersey Institute of Technology, Newark, NJ, 1992

- Bachelor of Science in Electrical Engineering, Drexel University, Philadelphia, PA, 1990

Major: Biomedical Engineering

Presentations and Publications:

Lacianca, Mark, Zimmerman, Mark C., Berndt, Hubert, and Parsons, J. Russell. "The Acoustic Properties of Bone Remodelling." Presented at:

- *New Jersey Orthopaedic Society*, Cayman Islands, March 1992
- *Fourth World Biomaterials Congress*, Berlin, April 1992
- *IEEE Northeast Bioengineering Conference*, University of Rhode Island, March 1992

ACKNOWLEDGEMENT

I would like to thank Dr.s J. Russell Parsons and Mark C. Zimmerman for their help over the last two years. Since my path to completing my thesis was not one that is, or should be followed, I want to extend special gratitude to Dr. Zimmerman for showing patience and in guiding my thesis to it's completion. I found the time I spent at the George L. Schultz Laboratory for Orthopaedic Research at UMDNJ to be rewarding, and although the final results were not exactly what was hoped for, alot of effort and hard work went into the research. The final results were still encouraging and leads me to believe there is a bright future for the field of scanning acoustic microscopy.

Appreciation is also extended to Tom Poandl and Alecia Marcantonio, whom I always found friendly and helpful. Finally, thanks to all of my fellow "ghetto" students who made the long hours of research as enjoyable as they could possibly be.

The completion of my Master's degree would not have been possible without the assistance of Dr. David Kristol. The Physic's Assistantship and the financial support provided from Ciba-Geigy, both of which Dr. Kristol played a large part in helping me attain, enabled me to attend New Jersey Institute Of Technology. I also found Dr. Kristol to be one of the better teachers that I have had throughout my college years, whose sarcasm made class enjoyable and also helped me in completing my thesis.

TABLE OF CONTENTS

LIST OF TABLES

Table **Page**

LIST OF FIGURES

CHAPTER ONE

INTRODUCTION

1.1 Bone (General Overview)

1.1.1 Anatomy

Bone is a dynamic material constantly growing and resorbing as a function of altered loading and stress states. If one were to look at a cross-section of bone through a high-powered microscope, one would see an ongoing process of demolition and formation of bone occurring at different stages. This is because the structural and mechanical demands on the skeleton are diverse. Some bones, such as the skull bones, have a primary function to protect internal organs from impact forces. Bone tissues at these sites, experience minimal repeated strains (or stresses) during normal daily activities. Bones of the lower extremity, on the other hand, usually experience thousands of cycles of loading and unloading everyday.

Bone exists in vertebrates only, and because of the diversity of bone it has many functions:

- mechanical support -- bone serves as a structural frame to support the body. The mechanical nature of bone extends beyond strength and stiffness, but also involves mechanisms by which the skeleton should not fracture or otherwise fail due to damage caused by repeated loading or fatigue fracture. These mechanisms are examined in more detail in later sections.
- locomotion -- bone enables movement by providing a point of attachment for the muscles providing a system of levers.

- protection of vital structures -- components of the axial skeleton (e.g. ribs, spinal cord, and the cranium as mentioned earlier)
- hematopoiesis -- bone houses the blood-forming system (red bone marrow), where red cells and platelets are being continually produced throughout life to replace aged cells.
- mineral homeostasis -- bone is the body's primary storehouse of Calcium and Phosphorous; 99 percent of the body's Calcium is in bone. Both of these minerals are vital to many body processes.

To examine bone more closely, the composition and structure of bone must be reviewed.

Bone is a hard extremely dense connective tissue, whose intercellular matrix consists of an organic component -- the fibrous connective protein collagen -- and an inorganic component -- crystals formed by the calcium, phosphate, and carbonate minerals. These two components are intimately bound, with the mineral crystals wrapped around and embedded among the collagen fibers. The hard mineral crystals provide great compressional strength, making bone an excellent load-bearing material. The collagen fibers add elasticity and high tensile strength, enabling bone to withstand tension forces. [1].

Most bones, and especially the long bones (such as the femur), are made up of two types of structure. The shafts are formed of compact (cortical) bone; the expanded ends, or epiphyses, usually include spongy (trabecular), or cancellous bone, with a thin cortex, or outer layer, of compact bone; this arrangement serves to transfer weight and stress from the shafts of the bones to the joints (see figure 1.1). The cortical bone forms the outer shell of a bone. It consists of a hard virtually solid mass made up of bony tissue arranged in concentric layers, called Haversian systems. The outer layer of the bone is called the periosteum, and the medullary cavity ("center of the bone") is lined with the endosteum and contains the marrow (inner cavity of the bone).

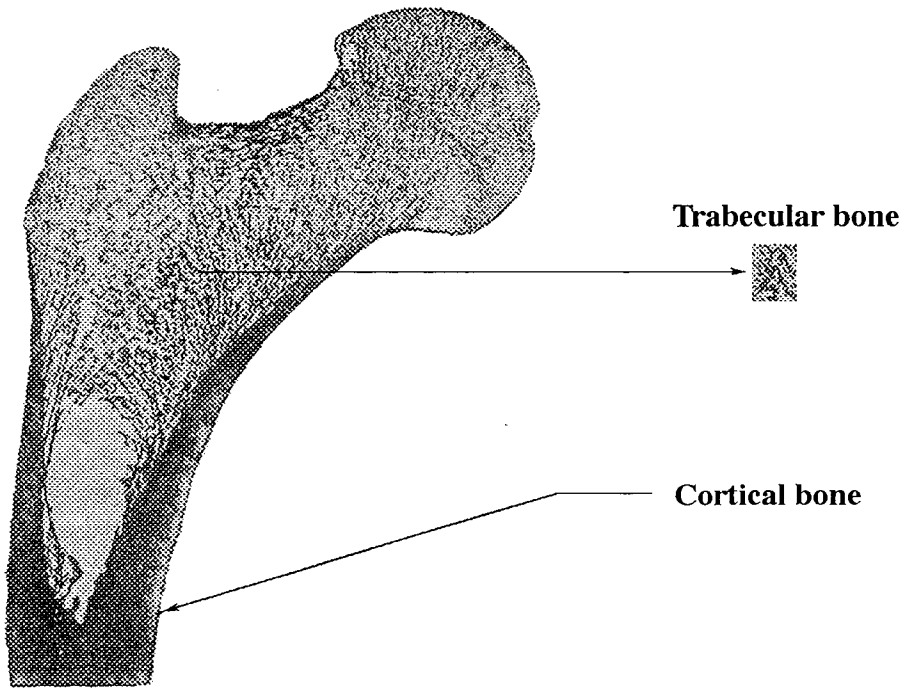

Figure 1.1 *Proximal Section of Femur*

The haversian system (or the osteon), is the unit of structure of compact bone. This is irregularly cylindrical and branching, with thick walls and a narrow central canal, carrying one or more small blood vessels. The haversian system is usually oriented in the long axis of the bone. The walls of the osteons are made up of concentric layers (or lamellae) of collagen and mineral crystals. The haversian system also contains a large number of lacunae which store the osteocytes (a type of bone cell that is discussed shortly), and are interconnected by a network of canaliculi, or minute canals. The canaliculi are the channels through which the fluids needed from the blood reach and nourish the bone tissue (see figure 1.2).

The living material of the bone, the bone cells, account for only 1 to 5 percent of the total bone volume in the adult skeleton. Bone cells are of four basic types:

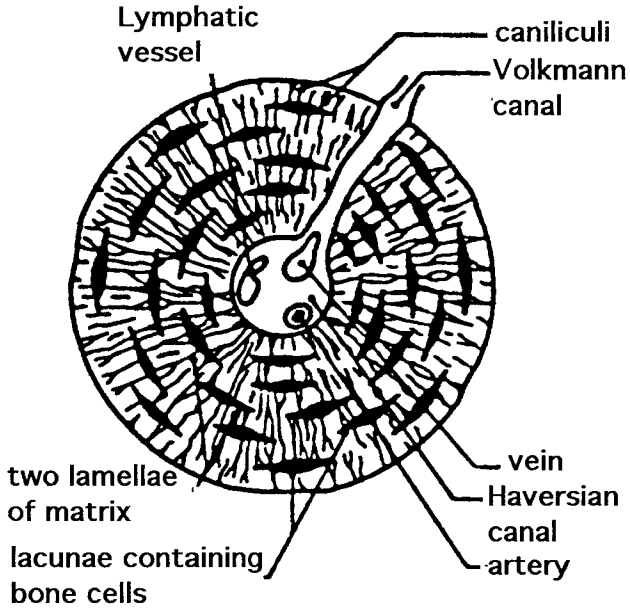

Figure 1.2 *Single Haversian System (or Osteon)*

(1) osteoblasts, are used to create new intercellular matrices.

(2) osteoclasts, resorb and destroy the original bone matrix.

(3) osteocytes, are derived from osteoblasts that have become embedded within the intercellular matrix, and serve to maintain the bone as a living tissue; and

(4) undifferentiated bone mesenchymal cells, which are located on the periosteum and within the internal spaces of the bone, and form new osteoblasts and osteoclasts.

These bone cells play a major role in bone remodelling. Bone remodelling, a process of destruction and regeneration, organizes immature bone into more orderly units that give the mature bone greater strength.

1.1.2 Remodelling

Bone has the unique quality of being able to remodel itself. The process is ongoing, where osteoclasts and osteoblasts are continually demolishing old bone and rebuilding it again. Resorption "crews", the osteoclasts, are the first to go to work. They destroy old bone tissue and create little cavities in the skeletal structure. The osteoclastic destruction that takes place within the bone helps to convert immature bone (often called woven bone) into mature compact bone by clearing long tubular spaces to serve as the center for the development of the osteon [see figure 1.2 of the single osteon -- previous section]. Next, the osteoblasts which are the builder cells fill in the empty spaces with collagen, a protein that is analogous to a concrete mix. Through a process known as "calcification", this collagen mixture will eventually harden (with the help of the hardening agent Calcium), and hence, new bone will be created.

Once this new bone has been formed, it undergoes a phase of remodelling, where old bone (or immature bone) is broken down and new bone forms. This generally occurs along lines of force, following Wolff's Law [2]. In this way the internal structure of bone changes so as to counteract the applied forces. Cortical bone is a living tissue which is continually adapting its geometry and microstructure to its mechanical environment. For this reason, any variation in the local elastic properties of cortical bone is directly related to its in-vivo mechanical load history. That is, bone mass can increase or decrease depending on the subsequent load (or lack of load), and is even susceptible to fatigue failure if the bone remodelling cannot meet the demands (or pace) of the bone resorption.

Mechanical loading appears to affect not only the gross and microscopic organization of bones, but their volume as well. These adjustments take place through the intermediary of the osteoclast and osteoblast populations involved in both modeling and internal reconstruction. It has been shown[3] (1) that bones tend to be more massive in individuals

(1) These studies tend to be focused on individuals who engage in very rigorous activities at an early stage of skeletal maturity. Hence, immature bone may have greater ability to respond to such loading than more mature bone. [4]

who have been physically active during growth. However, repeated loading of bone in everyday activities or prolonged exercise can lead to microscopic damage.

During fatigue loading, internal damage is created in the bone structure which causes a gradual and progressive loss of bone stiffness and strength prior to major, detectable crack formation. Normally, osteoclastic and osteoblastic activity (turnover) of bone serves to repair this damage and maintain the structural integrity of bone. Again, if damage accumulates faster than it can be repaired, fatigue fracture of bone may result. Fatigue fracture often occurs during prolonged exercise such as marching or long distance running [4]. However, a bone that is underutilized is unable to continue to strengthen itself. Examples would be a bone that is immobilized (as in a cast) or an astronaut in space (where loads are much smaller due to reduced gravitational fields), here the unutilized bone is prone to resorption.

1.1.3 Age/Osteoporosis

Aging plays a major role in the changing local anisotropic elastic properties of human cortical bone. In osteoporosis, a disease associated with the later stages of life (most common in Caucasian women over 50 [5]), the calcified mass of all bones decreases because bone resorption continues at a regular rate, while bone formation practically ceases, and thus demand exceeds supply. An example of an osteoporotic bone can be seen in figure 1.3(a), which shows a femur section taken from an individual with osteoporosis. For a comparison, figure 1.3(b), shows a similar section retrieved from a healthy femur. Both of these figures are displayed on the next page.

In the first three to four decades of life, osteoblasts are creating as much cortical and trabecular bone as possible. Cortical bones reach their peak mass (density) around age 35 to 40, and it stays fairly constant until about 45, when the cortical tissues begin to diminish.

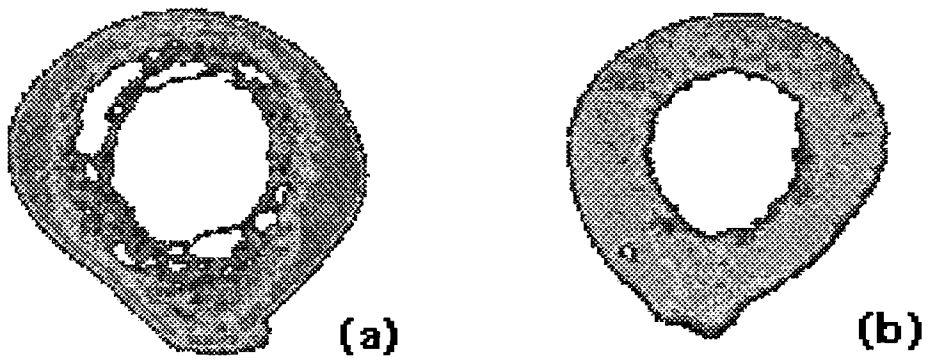

Figure 1.3 (a) and (b) *Two Femur Sections Scanned With the SAM. Section (a) Shows a Person Exhibiting Osteoporosis, while Section (b) Comes From a Healthy Femur.*

In contrast, trabecular bones reach their peak density at about age 25 to 30. After that, the trabecular bones in the back, ribs, and elsewhere begin a gradual decline in density that continues throughout life.

At about age 40, bone loss for both men and women proceeds at an annual rate of 0.3% to 0.5% of a person's total mass. Then, for Caucasian women who have just gone through menopause, bone loss may accelerate at a rate of 2% to 3% each year. This rate will normally decline after 8 to 10 years.

During their life spans, women lose about 35% of their cortical bone, and about one-half of their trabecular bone. Men lose nearly one-quarter of their cortical mass and about one-third of their trabecular bone [5, 6].

The pattern of age-related cortical bone loss involves thinning long bone cortices or cortical thickness loss with an accompanying increase in medullary diameter. The net age-related cortical thickness loss is achieved in spite of a gradual age-related increase in periosteal diameter in long bones [7, 8]. Concurrent with age-related cortical thickness loss is the loss of bone intracortically [9, 10]. Thus long bones not only become thinner with advancing age but also become more porous.

1.2 Analyzing the Remodelling of Bone

1.2.1 SAM - Reflection Technique

The Scanning Acoustic Microscope (SAM) is a reflection type microscope where the amplitude or the phase of the reflected sound wave is measured. Compared to conventional ultrasonic imaging techniques, which operate in the 1 to 10 MHz frequency range, acoustic microscopes can operate up to and beyond 1 GHz, where the wavelength is very short and the resolution correspondingly high. One would envision that the high frequencies would dominate the SAM applications. However, because of the high-attenuation properties of materials, the lower frequency range of 10 to 100 MHz is commonly used [11]. Many materials which are scanned acoustically, can easily be obtained with an optical microscope at a comparable resolution, with a great deal less preparation and expense. Therefore, the power of the SAM does not lie in its resolution alone. There are two advantages in using acoustic waves for producing images. The first lies in the ability of ultrasonic waves to penetrate materials that are opaque to other kinds of radiation, most notably light. In medical imaging use is made of the fact that ultrasonic waves can penetrate through body tissue, and can be weakly scattered by changes in the density or the elasticity of the tissue. The reflected echoes are detected and then are transformed into the scanned image (or acoustic impedance map). The second advantage of the SAM is the acoustic impedance map, which is able to show indirect contrasts in the mechanical properties (or elastic properties) of the specimen.

As mentioned earlier, the first practical SAM was developed and built in the early 1970's by Lemons and Quate [12]. A few years later Jipson and Quate [13], improved the SAM, enabling the microscope to obtain resolutions comparable to that of an optical microscope [optical resolution's limiting factor lies in the fact that there is a point at which the wavelength cannot become shorter -- approximately 400 nm]. The first SAM's were operated in the transmission mode, in which it was not necessary to use pulsed signals and

simple continuous wave electronics could be used. The first images were of biological specimens, where it was found that a contrast could be seen in the mechanical properties of the specimen without histological staining [14]. Interest began to shift from transmission microscopy to reflection microscopy, with a single lens being used for both transmitting and receiving the acoustic signal (which was now pulsed). There are two prevalent reasons for this. First, as the resolution continued to increase, the aligning of the two lenses became more difficult. The second, and more important reason, was the desire to image specimens of solid materials. Although acoustic waves are able to propagate through materials that are opaque to light, they will attenuate in any medium. Whereas. light can't penetrate opaque materials, but can travel through a vacuum with zero attenuation, and through air with very little loss. To minimize attenuation losses with the SAM, specimens imaged in transmission would need to be extremely thin. This stipulation can make it quite difficult to use the SAM in transmission and almost impossible for certain biological specimens. Therefore, the SAM has shifted most of its attention to the reflection mode, which is also the focus of this thesis.

Acoustic microscopes are practical tools that have emerged from the laboratory to find useful applications within industry. They can be applied to a broad range of problems that previously had no solutions, and they have been especially useful in solving problems with new high-technology materials and components not previously available. For example, in industry metallic samples can be used for non-destructive testing as well as for metallographic analysis with the SAM. The SAM also offers a technique for generating high-resolution images of material structure and defects in integrated circuits (IC's) located on silicon crystal substrates (silicon wafers are very important to the semiconductor industry). Without aid from acoustic microscopy, the metallic specimen would have to be polished and etched to reveal microstructural patterns, and the Quality Control which the SAM offers to the silicon wafers is unmatched by other devices [11]. Experiments have also been performed by the SAM on composite materials [15], animal cells [16], and even

to study living cells. For example, Hildebrand et al. [17] used an SAM operating at 1.7 GHz to study chicken heart fibroblasts, and found the microscope to provide a relatively direct means of studying the elastic state in localized regions within living cells. The SAM has been used in dental research, and the images show morphology that is equivalent to that of established techniques, but with additional information [18, 19]. Among other researchers, Meunier [20] and Zimmerman [21] have used the SAM in orthopaedic research. In a growing number of these situations it is being discovered that acoustic microscopy can provide new information, specifically about the elastic properties of a specimen at a microscopic level. For hard tissue analysis, this technique offers the advantage of nondestructive testing of a sample which can then be processed, enhanced, and further analyzed with other techniques.

1.2.2 Transmission Technique

The transmission technique uses ultrasonic sound waves, and typically operates in the 1 to 10 MHz frequency range. A major advantage of using this technique is its ability to obtain accurate physical properties of bone, such as the Modulus of Elasticity, in a non-destructive manner. This can be accomplished by using ultrasonic energy, when it is transmitted through a material it applies stresses to the particles of the material and this mechanical energy is affected by the elastic behavior of those particles. It is commonly known, that the velocity of an ultrasonic wave through a material is dependent on the Modulus of Elasticity of that material and its mass density. This relationship is expressed as:

$$\text{Velocity} = \sqrt{\text{Modulus of Elasticity/Density}}$$

This formula is derived for "purely" elastic materials, and should be applied cautiously to visco-elastic materials, such as bone (see figure 1.5) [22]. The Modulus of Elasticity (or

the C_{33} value) can be calculated by using the transmission technique to measure the velocity of ultrasound through bone and the density.

In orthopaedic research, transmission ultrasonic techniques have been used since 1970 to measure the anisotropic elastic properties of calcified tissue [20] - [27]. Yoon and Katz [28] derived the equations relating the elastic constants to the technical moduli. Some investigators have even used these techniques to determine the different mechanical properties of pathological bone (osteopetrotic, osteoporotic) [29]. Abendschein and Hyatt [22] demonstrated that there was a good correlation between the longitudinal modulus (E_3) measured by using ultrasound and mechanical techniques. Different investigators have used the transmission technique for measuring the ultrasound velocity within the specimen. Yoon and Katz studied ultrasonic wave propagation in dried normal human femoral cortical bone at room temperature at 5 MHz [30]. This can be accomplished by placing the specimen between two transducers (in our case, 5 MHz), one a transmitter and the other a receiver. Knowing the distance between these two transducers, and the time for the ultrasound to travel through the specimen, the velocity is determined. Given the geometrical orientation of the specimen, it is possible to determine the elastic constants (Young's modulus) in all three space orientations [31]. Yoon and Katz [26], Lang [24], and Van Buskirk and Ashman [32] have made significant contributions regarding the use of ultrasound to measure material properties, and in determining the properties of bone.

The importance of correlating the SAM to the ultrasonic transmission technique was shown by Meunier et al [25]. Meunier found a high correlation between the data obtained using transmission and reflection techniques. Using the transmission technique, they measured the elastic stiffness in 30 different femur specimens. They also measured the acoustic reflection and impedance from the same specimens. They compared this data and found a correlation factor of 0.99 as illustrated in figure 1.4 (next page). Meunier's work demonstrates an "almost perfect" correlation between the elastic stiffness and an acoustic property of bone. This finding allows the orthopaedic investigator to use the terms elastic

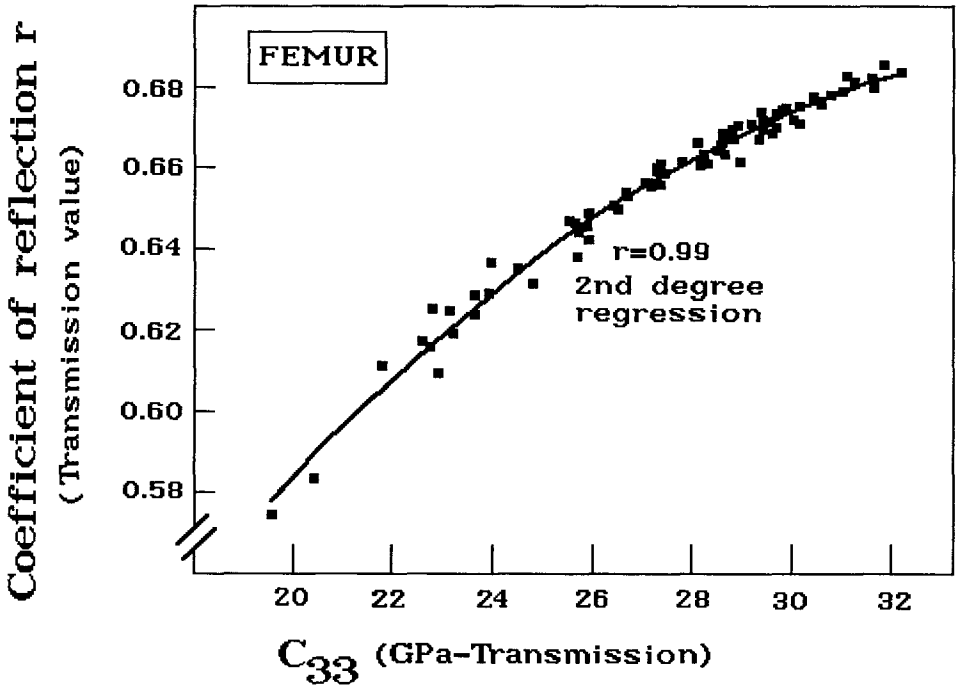

Figure 1.4 *Correlation Between the Elastic Stiffness and the Reflection Coefficient (R) of Bone Measured With an Ultrasonic Transmission Technique*

properties and elastic constants almost interchangeably, because of the correlation shown between the two techniques. This is very important, because this relationship is not true for all materials. The importance of the SAM will be seen in the acoustic impedance map, which allows one to see the material properties on a much smaller scale than the transmission experiments.

1.2.3 Mechanical Testing

Non-destructive mechanical testing of bone, allows an investigator to compare the elastic constant data from compression testing to that of another technique (SAM and/or Transmission). As with all structural materials, when bone is subjected to external forces, it generates an intermolecular resistance to the deformation [33]. A measure of this capacity to resist deformation is Young's Modulus. This modulus is defined as the ratio of stress to strain. Stress is defined as the force per unit area (units are Newtons/mm^2). Strain is the

measure of the deformation caused by that force. It is measured as the ratio of the change in dimension of the test object (i.e. bone cube) to its original dimension.

By means of the Modulus of Elasticity and analysis of the stress/strain curve one can predict quite precisely the behavior of the material under various conditions of stress. However, bone is heterogeneous, anisotropic, and viscoelastic [22]. In addition, all of the bone tested from this thesis experiments comes from cadavers over the age of 75, and therefore osteoporotic bone plays a major role in the stress/strain curve. Only in an ideally elastic material will the Modulus of Elasticity be expressed in a pure linear relationship of stress to strain. Thus, even prior to reaching the elastic limit of bone, the stress/strain ratio is not purely a linear one and the Modulus of Elasticity might best be considered as a "tangent modulus" or the slope of the tangent line measured during the elastic phase (see figure 1.5).

Even with these limitations, the Modulus of Elasticity for bone gives one invaluable information about bone's behavior when external stresses are applied to it. The modulus has been correlated with the breaking stress in standardized specimens of human femurs by Sedlin and Hirsch [34] and intact femurs by Mather [35]. Thus, it might be conceivable by

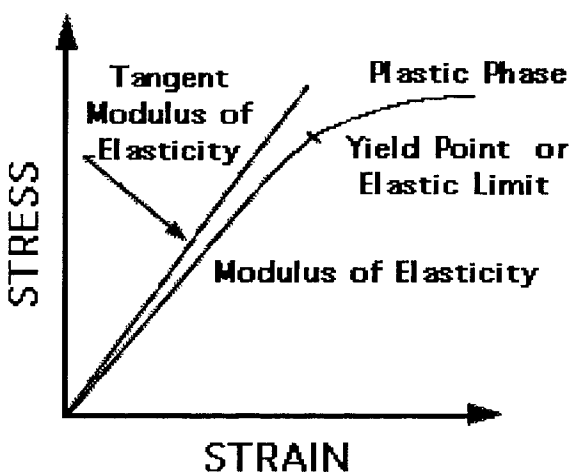

Figure 1.5 *Stress/Strain Curve for Cortical Bone*

means of non-destructive measurement of the Modulus of Elasticity of bone to accurately predict the breaking strength of that bone. More importantly to this study, Young's Modulus is directly correlated with the C_{33} value determined from the transmission technique, thereby giving another set of data to verify the accuracy of the SAM results.

1.3 Rationale

Bone is a unique material that constantly rebuilds and remodels itself in response to mechanical stresses. To understand how bone remodels, one must be able to measure the elastic properties on a microscopic scale. Scanning acoustic microscopy may be the only technique where this is possible.

Mechanical testing, the standard and most often used technique for analysis of the material properties of bone, only allows for a relatively large section of bone to be tested (smallest size approximately $10mm^2$). Histological techniques have also been used in the analysis of bone. Hard tissue histology provides detailed information concerning distribution of cell type, cellular activity, and bone volume. Backscatter scanning electron microscopy provides sharp tissue boundaries and high tissue contrasts. These histology techniques provide high resolution information regarding bone, however, the information is of a qualitative nature. Now, one is left with "quantitative" elastic modulus data on a gross scale provided from mechanical testing and "qualitative" materials property information that is found using histological techniques. The SAM can provide both, elastic constant data on a microscopic scale and a qualitative "picture" of an entire bone section.

The SAM has already shown its usefulness in industry. The aerospace industry has used imaging for over 30 years on parts that are heavily stressed for subsurface cracks, voids, and delimitations in materials where these features are undetectable optically or by any other means currently available [36]. Non-destructive mechanical testing is a major reason the SAM was used for analysis in industry. By using acoustic microscopy on bone

specimens, quantitative and qualitative information could be retrieved, and the undamaged bone could be used for alternative analysis.

The SAM has already shown a potential use in the design of better orthopaedics implants and in determining the strengths and weaknesses of "different types" of prosthesis (i.e. an uncemented prosthesis vs, a cemented prosthesis) which have and currently are being implemented [21]. This is extremely important in todays' society where joint replacement has become a frequent treatment in orthopaedic surgery for patients with severe arthrosis, rheumatoid arthritis, or other possibly disabling conditions. For example, in 1982 65,000 patients received a new prosthetic hip in the USA alone [37]. One decade later, that number has reached 500,000 and with the aging American population the number of hip replacement surgeries performed should only increase.

The great interest in bone remodelling is largely a product of the clinical observations of the long-term response of bone tissue to the presence of orthopaedic implant devices. Stress shielding at the proximal end of the femur has been identified as a possible cause of the long-term loosening of prosthetic hip replacements [38]. The attachment of high modulus metal bone plates has been shown to result in a reduction of bone mass in the diaphysis of the plated bone [39, 40]. On the other hand, studies have shown that osteogenesis can be stimulated by increasing stress [41]. These clinical and experimental findings have demonstrated the need to characterize the relationships between the morphological and mechanical properties of bone and the stress history that it experiences. With a more complete understanding of this relationship, improvements could be made in the design of prosthetic implants, which in turn would enhance prosthetic attachment by maintaining healthy tissue and/or promoting osteogenesis. The SAM with its ability to analyze a cross-section retrieved from a cadaver that has undergone a hip replacement would be a very powerful tool. After retrieval of a specimen a bone could be analyzed at different section locations. This data could then be entered into an FEM software package to obtain a more accurate model of a prosthetic hip device.

There are still many untouched areas in orthopaedic research where scanning acoustic microscopy can have a significant impact. First, embedded specimens can be analyzed for materials properties information, where it is believed that bone can be measured relative to the properties of the embedding medium (plastic). This has global ramifications, since every piece of bone ever embedded in plastic could be reexamined for materials properties analysis. Secondly, for certain irregularly shaped areas it is impossible to measure the mechanical properties of bone either because of size or the irregular geometry. Facet joints in the spine and the insertion sites of ligaments are prime examples. This technique could be used to assess changes in spinal, ligament, or biomechanics that would affect their respective structures. Finally, acoustic impedance maps can be presented on a microscopic scale replacing gross measurements over a larger area of bone. Differentiation of endosteal vs. periosteal remodelling, different bone types and their properties, and effects of different disease states on the properties of the bone will be possible. Scanning acoustic microscopy is the only technique available that has the capability to perform these applications.

A major purpose of this thesis was to validate the correlation between the acoustic impedance maps obtained from the SAM, to the corresponding Z (acoustic impedance) numbers retrieved from the ultrasonic transmission technique. By proving that the SAM is a useful orthopaedic tool, as shown above the microscope will enhance many areas of orthopaedic research. The experiments involved using the acoustic microscope assembled in our lab to scan 30 cross-sections procured from five pairs of human femurs that have no history of an orthopaedic device being implanted. Further, these whole sections were cubed into 120 quadrants, which in turn 40 of these reduced areas were scanned. The ultrasonic transmission velocity was found from these cubes and compared to the SAM values. A second aim of this thesis, was to examine the effect histological procedures (the embedding of specimens in polymethylmethacrylate) have on the ability of the SAM to collect accurate results. The embedding process is in common use in many laboratories

throughout the United States, and the realization that reliable data can be collected from these samples would be extremely important to orthopaedics.

CHAPTER TWO

MATERIALS AND METHODS

2.1. Bone Preparation

Eight pairs of human femurs were obtained from cadavers that had no history of orthopaedic device implantion. The femurs were sectioned transversely with a low-speed diamond saw and saline was used to cool the blade. The position of each transverse section was taken at the same location relative to the greater trochanter. They were cut into three pieces, and each was approximately 10 mm in length. The thickness of the slice must be at least larger than several times the wavelength of the ultrasonic wave (0.5 mm in 30 MHZ and 0.3 mm in 50 MHz) in the tested material so that the echo generated at the back surface does not interfere with the main echo produced at the upper face. As shown in figure 2.1 (next page), the three sections were removed from the mid-shaft of the femur and labelled distal, middle, and proximal according to their anatomic location to the trochanter of the femur. From the original eight pairs, three pairs were eliminated because the level of osteoporosis was extremely high as assessed by low power light microscopy. Therefore, five pairs of femurs were used in this experiment.

To prepare each section, a custom designed grip was used to obtain parallel faced specimens (currently, the parallelism is better then 10 um for a 900 mm^2 area specimen [6]). The slice is then polished with a 1.0 um alumina slurry, on an 8 in. diameter bronze wheel covered with a polishing cloth. An optical reflection microscope is used to examine the quality of the polishing as well as to detect any defects or cracks that would affect the acoustic measurements. Thus, once the specimen is aligned in the instrument, the parallelism assures that the wave front is always perpendicular to the specimen. Finally, each section was placed in an ultrasonic cleaner for 5 minutes to clear the bone of any "grit" that may have entered during the sanding process.

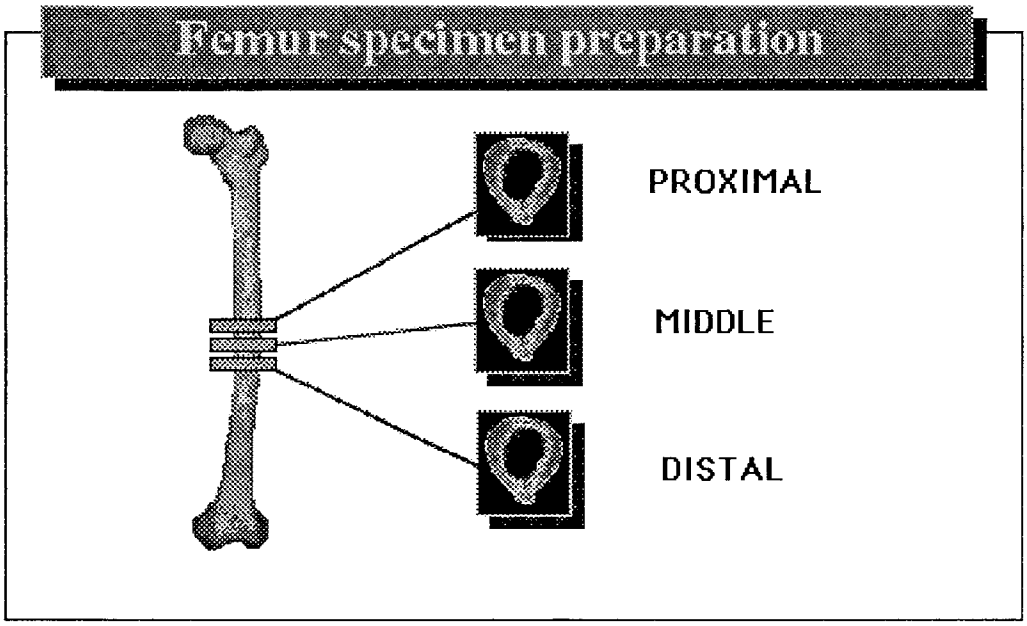

Figure 2.1 *Three Sections from the Midshaft of the Femur*

2.2 Scanning Acoustic Microscope (SAM)

The 30 "whole" sections, which have now been processed and are parallel, were used with the scanning acoustic microscope (SAM) reflection system to obtain an acoustic impedance map of each section (30 MHz transducer). The acoustic impedance for the sections was determined with a circular averaging program, to be described in section 2.2.4. The acoustic impedance is significant because it provides a direct measure of the elastic properties of bone. While not being directly a technical engineering modulus, the acoustic impedance is in itself a material property, which can provide valuable information about inhomogenities in materials' behavior, especially across interfaces. The equations for the acoustic impedance and elastic stiffness in the same directions are:

$$Z_i = \rho v_i \quad (1)$$

$$C_{ii} = \rho v_i^2 \quad (2)$$

$$C_{ii} = z_i v_i \quad (3)$$

where ρ = density of bone, v_i = velocity of an acoustic longitudinal wave through bone in direction i, z_i = acoustic impedance, and c_{ii} = elastic stiffness in direction i. Thus, if either ρ or v_i can be ascertained independently at each pixel location on the specimen, it would be possible to obtain a map of the axial elastic stiffness coefficients, C_{33}, comparable in resolution to the maps of z_i itself.

The SAM system can be divided into four main parts: (a) the acoustic equipment, (b) the scanning system, (c) the computerized data acquisition and analysis apparatus, and (d) the calibration and error analysis. A schematic view of the system is presented in figure 2.2

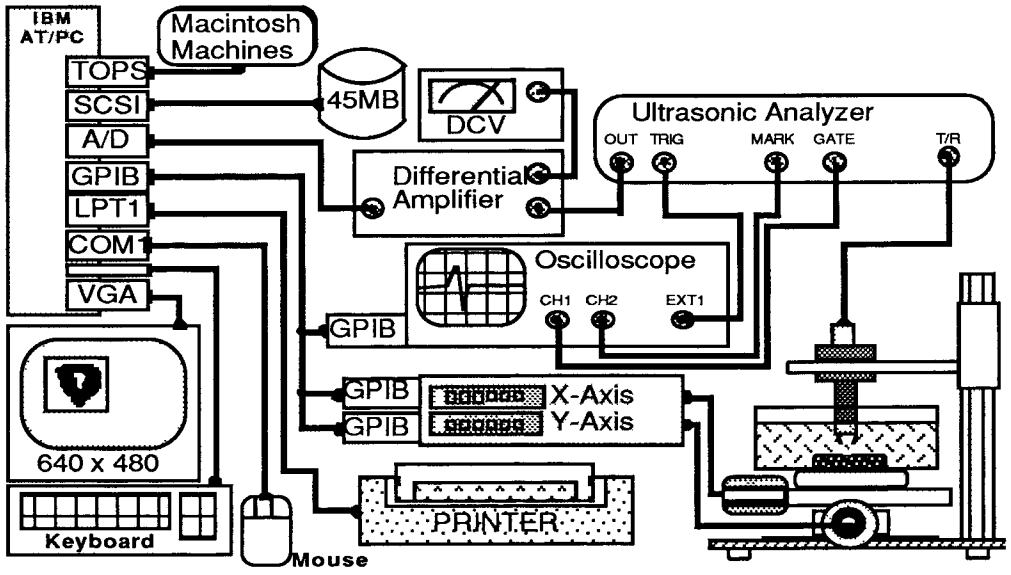

Figure 2.2 *Schematic View of the Scanning Acoustic Microscope (SAM)*

2.2.1 Ultrasonic Equipment

A generator, which is produced from the ultrasonic analyzer[2] (model 5052-UA), delivers electrical pulses with a repetition rate ranging from 100 Hz to 5 KHz to a piezoelectric

(2) Panametrics Inc., Waltham MA

transducer that transforms the electric signal into an acoustic wave. A polymethylmethacrylate (PMMA) lens spherically focuses the ultrasonic pulse (focal length = 25.4 mm). A part of the acoustic pulse is reflected back to the transducer, which this time acting as a receiver, transforms the acoustic echo into an electric pulse. The amount of sound reflected is directly related to the acoustic impedance of the material. This pulse is then transmitted to an electronics unit, which conditions the signal. Finally, the amplitude signal is then adjusted to the voltage range of an analog/digital converter through a differential amplifier. An oscilloscope is used in order to visualize either the entire pulse signal or just the peak amplitude signal.

The original ultrasonic transducer that was used in this apparatus had a frequency of 30 MHz. The size of the acoustic spot in the lens focal plane was approximately 100um. The focal point is not truly a point, but an acoustic amplitude distribution that follows a Bessel function (the width of the principal peak is approximately 100um for a 20 MHz transducer).

2.2.2 Scanning System

In order to obtain multiple measurements on the surface of the specimen, the sample is mounted on a special holder that is fixed in a small tank mounted on an X-Y table system. Each table can be translated using a stepping motor (one rotational step induces 10um of translated motion on the X or Y stage). The X-Y displacement is driven either manually (initial positioning of the sample) or driven and controlled by a Programmable Stepping Motor Controller CC 1,2 from Klinger ® Corp. that can communicate with other devices through a GPIB-bus, RS-232 port or a non-standard parallel communication port. This non-standard communications port provides important signals and information about status of run, speed, actual position from front display or even the control pulses to the stepping motor. The stages can be moved in single steps or in continuous movement with different speeds, accelerations, and decelerations. The speed of each displacement can be adjusted

independently between 1 and 20 mm/s. Depending on the weight of the tank, its load, the image size to be obtained and the required kinematics of the system, different movement characteristics have to be initialized and assigned to the controller.

The acoustic transducer is mounted on a rigid column in the Z-direction (vertical) and a micrometer is used to raise or lower the transducer in order to achieve the focusing of the signal onto the specimen surface. Special attention has been given to assure the perpendicularity between the acoustic transducer transmission direction and the specimen surface.

2.2.3 Computerized Data Acquisition and Analysis Apparatus

An IBM-PC controlled the apparatus. This microcomputer performs three functions:

(a) Driving the scanning of the specimens. This scanned area can be varied from 6.5 to 1300 mm^2 and consists of 256 consecutive lines. A complete scan takes approximately 5 to 15 minutes depending on the size of the areas to be analyzed.

(b) Simultaneously performing the data acquisition process of the amplitude signal through through a 12-bit Analog to Digital (A/D) converter which is part of a data acquisition board (model 5525MF from ADAC Corp.). The maximum speed of the data acquisition of the A/D converter is 25 KHz. Considering the relatively slow speed of the mechanical scanning, about 6000 measurements are obtained along a single scanned line. 256 of these values are stored on a disk, and saved at equally spaced positions, resulting in an array of data with 256 rows and 256 columns (65,536 data points).

(c) Software specially developed for this application allows presentation of the scanning results as a pseudo-color mapping of the data (16 colors can be used on a 640x400 pixels' screen). This 2-dimensional map can be zoomed up to 16X magnification in order to enhance areas of special interest. The software was also capable of changing the color/gray level values and its distribution according to a histogram. A single color generally covers a range of acoustic impedance values, therefore, some important details may be lost. Thus

the software also provides for presentation of a pseudo 3-dimensional image in which the amplitudes are presented directly as measured in the same pseudo-color scheme as on the 2-dimensional map. A single scanned line (one of the 256 making up the pseudo 3-dimensional image) can also be plotted in profile.

Iso-acoustic impedance lines can also be plotted as an aid to visualization of the distribution of property values throughout an area for comparison with optical studies and histomorphological evaluation.

2.2.4 Data Processing

Once the data is sampled and stored on a disk, it can be read, processed, and presented on the screen by using a program for image processing and evaluation. The acoustic impedance, for the initial 30 sections that were scanned, was found using software developed by Meunier and enhanced by Berndt [42]. Over the course of the nine months in which these experiments were performed, Berndt developed a second program that was used to scan the 39 embedded bone cubes. A brief description of the two programs is presented:

(a) Meunier wrote the initial image analysis software in Turbobasic. Once the image was stored, a variety of functions could be performed. For example, the color distribution could be selected to modify the 16 color (or gray level) histogram distribution, the area of an object could be computed, or an image could be presented 3-dimensionally. More importantly, the program computed the elastic properties with respect to the location on the object. The center of gravity was found and broken into three regions - the outer-third, the middle-third, and the inner-third and the entire section is investigated in 10° increments and proceeds with a circular weight averaging. This allowed the user to analyze a tubular bone section (i.e. a femur) in the endosteal, middle, and periosteal regions. Finally, the program calculated the average arbitrary ultrasonic impedance values for each of these regions, as well as the average value for the entire section with each region carrying equal weight.

(b) The second program was developed by Berndt, and written in Turbo C++. This software was written to be user friendly, and allow the user more freedom in determining the acoustic impedance. The program has all of the capabilities that Meunier's possesses. In addition, the use of the mouse allows one to determine a specific area (with the limitation being that the area selected be rectangular in nature). In turn the program presents the acoustic impedance and size (in mm^2) of that area. The entire bone may also be selected. The acoustic impedance was not calculated with this program in terms of three regions. The impedance calculated is the averaged value of all the impedance data from the area of bone which is selected (the entire bone scanned may be selected).

2.2.5 Calibration and Error Analysis

As described above, the signal voltage, which represents the value of the voltage corresponding to a given acoustic impedance (value of Z), as recorded by the receiver is given by:

$$V = \alpha (V_R + \beta) \qquad (4)$$

where α and β are variable parameters determined by setting the electronics and V_R is the voltage recorded by the transducer in its receiving mode. As with optical systems, this analysis "assumes" that the focal point is infinitesimally small at the specimen surface, and that the entire surface of the specimen is located exactly in the acoustic focal plane. Figure 2.3 (next page) shows the relative error which will be introduced in this amplitude measurement when the specimens surface is out of the focal plane. In order to assure that this error is less than 0.5% it is imperative to maintain the specimen surface within 80um of the focal plane.

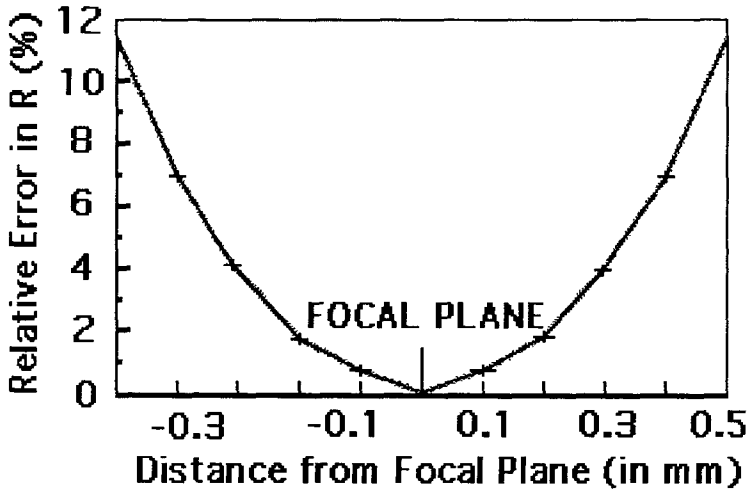

Figure 2.3 *Relative Error Introduced when the Specimen Surface is Out of the Focal Plane*

To demonstrate the out-of-focal plane effects shown above, Meunier [43] and Berndt [42] used the SAM on a standard American quarter (see figure 2.4, next page). Here, the material is uniform throughout the coin; however, all the detailing --- motto, date, head, etc. --- is raised above the flat background, which was located in the focal plane. Thus any amplitude variations observed are not due to changes in the material properties, but are due instead, both to deviations from the focal plane and the edge effect. The edge effect is due to the fact that the focal point is not truly a point, but instead has an acoustic amplitude distribution which follows a Bessel function (width of the principal peak is approximately 100um for 20 MHz transducer).

Under the assumption of perfect focusing, $V_R = V_I \cdot R$ where R is the reflection coefficient at the point being measured and V_I is the voltage emitted by the transducer in its transmitting mode, so that $V = \alpha (V_I + \beta)$. For a specimen immersed in water, its value of R_S for the specimen is given by:

$$R_S = (Z_S - Z_W)/(Z_S + Z_W) \qquad (5)$$

Figure 2.4 *SAM Image of U.S. Quarter*

where Z_S is the acoustic impedance of the specimen at the point being measured and Z_W is the acoustic impedance of water. Thus the value for the reflection coefficient for water, R_W, in this case is zero. With the transducer in the water bath, but not over the specimen, the electronics are adjusted so that the voltage recorded is some value V_W. Therefore, $\alpha\beta = V_W$. The transducer is now aimed at a material that is chosen because of its homogenous nature and it is easily reproducible (a common slide used for histology procedures), whose acoustic impedance Z_P, and therefore whose reflection coefficient, R_P, is known. In this case the electronics are tuned so that the voltage $V_P = 0$. Thus $(V_I \cdot R_P + V_W/\alpha) = 0$ or $\alpha = -V_W/V_I \cdot R_P$. When these are substituted back into equation (1), the relationship between the acoustic impedance at a point in the specimen and the voltage recorded at the receiver is established and quantified in a simple relationship:

$$(V_S/V_W) = 1 - (R_S/R_P), \text{ or } (R_S/R_P) = 1 - (V_S/V_W) \qquad (6)$$

However, since it is Z_S, the acoustic impedance of the unknown specimen at a point, which is eventually desired, equation (3) is "rewritten" with R_S replaced by equation (2) to obtain:

$$Z_S = Z_W \cdot [1 + R_P(1 - V_S/V_W)]/[1 - R_P(1 - V_S/V_W)] \qquad (7)$$

To calibrate the SAM in our laboratory, a second material was chosen, e.g. glass, again a material that is homogeneous and easily reproducible. Glass and Plexiglass, were also chosen because their acoustic impedances are above and below bone, respectively (see figure 2.5). To guarantee that consistent quantitative data could be reproduced from bone scans, the same "calibration sample" was scanned at the beginning of a days scanning, which contained a piece of glass and plexiglass embedded in polymethylmethacrylate (PMMA) and was polished parallel. At the completion of scanning the "calibration sample", the known acoustic impedance values were set for glass and plexiglass (Z = 13.62 and Z = 3.23, respectively) using specially designed software. Thereby, allowing a consistent procedure to gather data. Assuming there is a linear acoustic impedance region between glass and plexiglass (again see figure 2.5 (a) and (b)), and using the general equation y = mx + b, an acoustic impedance value could be obtained for any specimen whose acoustic impedance was between 3.23 and 13.62 (i.e. bone).

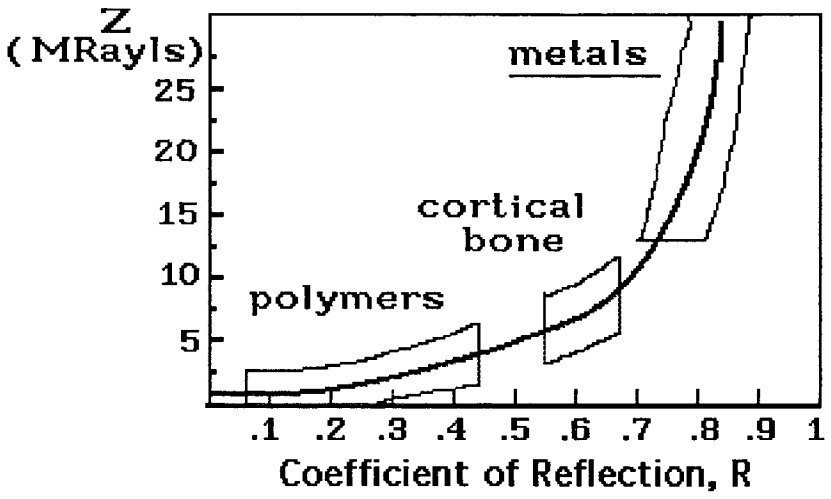

Figure 2.5(a). *Reflection Factor (R) and Acoustic Impedance for Various Materials*

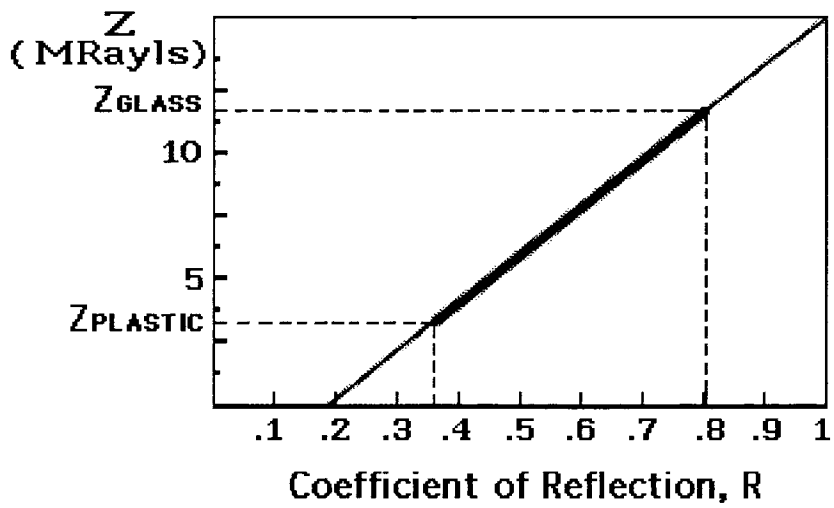

Figure 2.5(b) *The Theoretical Acoustic Impedance Between Glass and Plastic*

2.3 Cubed Bones

Once the 30 "whole" sections were scanned, each section was cut using the low-speed diamond saw into four rectangular parallelopipeds (see figure 2.6) approximately 5x5x10 mm thick, one from each of the four aspects: anterior, posterior, medial, and lateral. Each

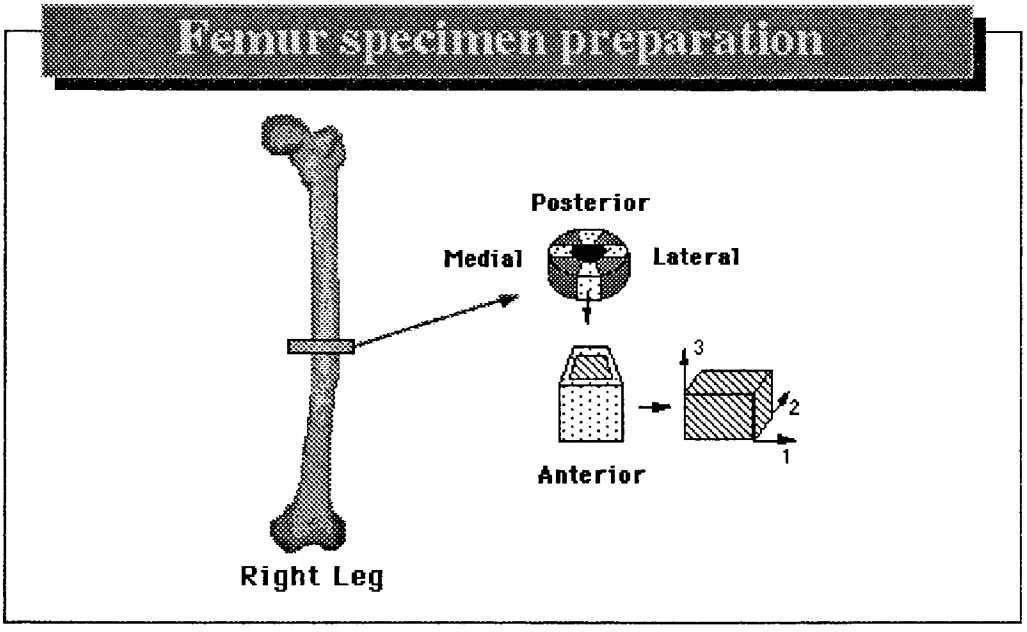

Figure 2.6 *The Sectioning of Bone into Four Quadrants*

piece was cut such that the predominate direction of the osteons' axes was parallel to the long axis of the sample (X_3) as determined by reflection light microscopy. These 120 cubes were used to determine the elastic properties using an ultrasonic pulse-through transmission technique.

2.3.1 Acoustic Velocity Measurements

The ultrasonic test system (shown in figure 2.7 - next page) consisted of two 5 KHz plane-wave transducers with a focal length of 25.4 mm, a Panametrics ultrasonic analyzer (model 5052-UA), and a Tektronix oscilloscope. Distilled water was used as a coupling material, and contact between the transducers and the bone cube was formed with light contact

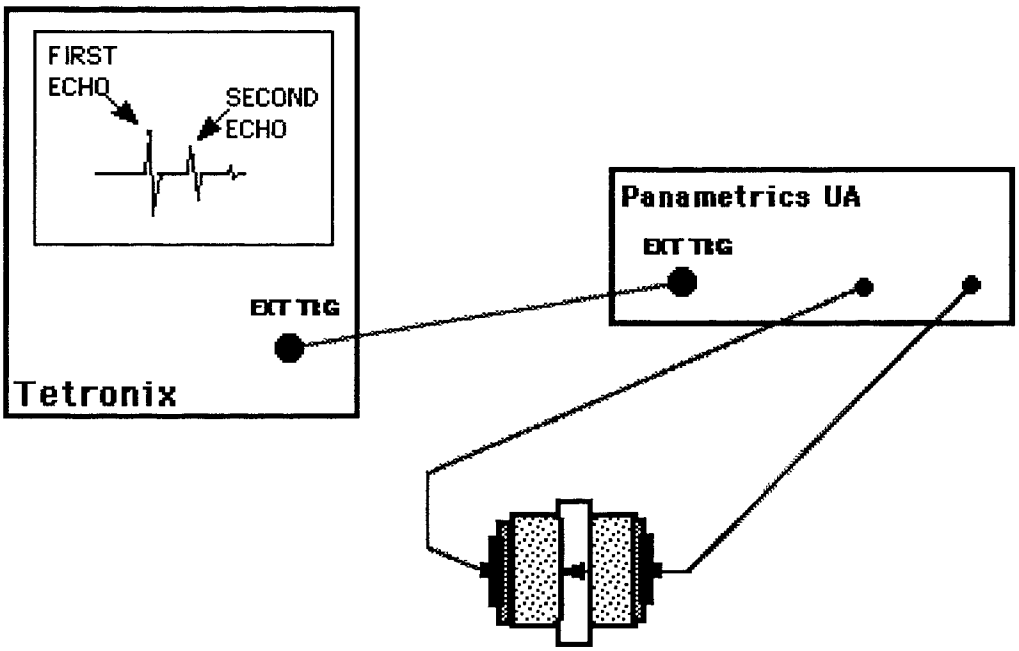

Figure 2.7 *Schematic of Ultrasonic Testing System*

When the ultrasonic wave passed through the bone specimen and reached the receiving transducer, the mechanical sound energy was converted to electrical energy which can be seen on the oscilloscope. Pulse transit times or delay times in the specimen were measured

from the shift in the relative positions of the pulses without the specimen as observed on the horizontal axis of the oscilloscope. The transit time divided by the length of the specimen gives the average velocity of ultrasound in meters per second (V = distance/time).

2.3.2 Density Measurement (water immersion technique)

The density of bone was determined by weighing each specimen on an Ainsworth Type 10 N analytical balance. The specimens are then weighed while being completely submerged in distilled water. The apparent loss of weight in water, due to the change in density from air to water, is subtracted from the original weight of the specimen and divided by the density of water (which is assumed to be 1). The original weight of the specimen in air is divided by the result obtained above to give the mass density of the specimen being investigated:

$$\text{Density (kg/m}^3\text{)} = \frac{\text{Weight in air (kg)}}{\text{Change in weights / density of water (kg/m}^3\text{)}} \qquad (8)$$

2.3.3 Elastic Property Measurements

Using the ultrasonic velocity density measurements, the elastic properties can now be determined as shown earlier. The acoustic impedance is the product of the density, ρ, and the longitudinal velocity, v, i.e., $Z = \rho v$. Clearly, Z is closely related to the elastic stiffness coefficient C_{ii} measured in the same direction, e.g. for the principal mode direction along the bone axis $C_{33} = \rho v^2$. Determining the acoustic impedance, Z, using the transmission technique is very important for two reasons:

(a) The technique has been proven very accurate and is easily reproducible, and

(b) The accurate acoustic impedance from the transmission technique allows the investigator to determine the accuracy of other methods, in this case, the SAM.

2.3.4 Mechanical Testing

At the completion of the Transmission testing on all 120 cubes (40 each from the distal, middle, and proximal sections), the 40 proximal cubes were then non-destructively tested on an MTS servohydraulic mechanical test system. The remaining 80 cubes were saved for future experiments. The cubes which were approximately 5x5x10 mm were tested in compression to determine Young's Modulus (E), the formula is:

$$E\ (N/mm^2) = \frac{\text{STRESS } (N/mm^2)}{\text{STRAIN}} = \frac{\text{Force/Area}}{\text{Deformation to the original shape}} \qquad (9)$$

2.4 Histology

At the completion of the mechanical testing on the fresh proximal cubes, standard histological procedures were followed. Each cube was dehydrated in a series of ethanol (40% - 100%), cleared with Hemo-De, and embedded in hard PMMA. The embedding schedule is explained in its entirety in figure B.1 (Appendix B). The cubes were then further reduced to approximately 5x5x3 mm sections using the low-speed diamond saw, and the "superior" side was polished. Again a parallel surface is extremely important, before the SAM can be used.

2.4.1 Scanning Experiment (50 MHz)

For reasons which will be discussed later, the SAM was now operating at 50 MHz. In turn, the size of the acoustic spot in the lens focal plane was approximately 75 um. The 39 proximal sections (one was destroyed during the mechanical testing) now embedded in PMMA were scanned, and analyzed for their acoustic impedance values. The acoustic impedance was determined, as shown earlier, for the cubes and the PMMA.

CHAPTER THREE

RESULTS AND DISCUSSION

The transmission and SAM experiments described previously were performed in our laboratory over a period of twelve months. During this time, improvements were made on the SAM, and changes were made to the bone that was being tested (i.e. sectioning of cubes from cross-sections and the PMMA embedding process). Therefore, it is extremely difficult to make comparisons between results from the earlier scans and the results from the final scans. For the above reasons, as well as simplicity in presenting the data, the data and a majority of the discussion on the data is being presented in four separate sections.

3.1 Elastic Constant Data

As discussed in the Materials and Methods section, the density of bone and the velocity of an acoustic wave through the same bone section are acquired in order to calculate the elastic constant data (Z and C_{33}). To restate the equations for reference:

$$Z_i = \rho v_i \tag{1}$$

$$C_{ii} = \rho v_i^2 \tag{2}$$

$$C_{ii} = z_i v_i \tag{3}$$

3.1.1 Velocity and Density

The data for the 120 bone cubes tested with the ultrasonic transmission technique and the water immersion technique are presented in Tables 1A and 2A (Appendix A), respectively. The values obtained from these experiments are comparable to other orthopaedic investigators [3, 5, 6, and 54], and it can be seen that the dilational velocities for each quadrant are slightly higher (0.1 +/- 0.05) than the values that Meunier obtained.

By using statistical analysis, conclusions can be made on the significance of the data. Paired t-tests (left vs. right) proved, as expected, that there were no significant differences

By using statistical analysis, conclusions can be made on the significance of the data. Paired t-tests (left vs. right) proved, as expected, that there were no significant differences between either leg ($p<0.05$). More importantly, no significant difference was found between the three sections taken from the femur (middle, distal, proximal). This proves that consistent data can be obtained, at a gross level, over a 3 cm range even with older bone. It is commonly known that bone becomes more porotic and less homogenous with age, but the data show that even the bone of the elderly (75 years of age) still has a remarkable amount of consistency within it. However, the orthopaedic investigator should attempt to retrieve femoral sections from the same region of the femur (i.e. midshaft), since the porosity in each quadrant (especially in the anterior and posterior) changes over the entire length of the femur [32 and 43]. Scanning acoustic microscopy may complement the transmission technique, and show inhomogenities in the elastic properties at a microscopic level. Finally, a statistical difference was found when comparing the posterior section to the other 3 quadrants (unpaired t-test, $p<0.05$). In both techniques, transmission and water immersion, the posterior region was significantly lower compared to the other quadrants.

Figure 3.1 (next page) graphs the entire range of velocity data collected with the transmission experiment and plots it against the corresponding density values. In theory, a bone that is more dense will have less voids and therefore be more homogeneous allowing an acoustic sound wave to travel faster. Conversely, a bone with a lower density, will have more voids, and since sound travels faster through bone or water as compared to air, the velocity of the sound wave will be slower. The correlation factor ($R=0.733$) found from figure 3.1 and in previous work ($R=0.866$ - [22]) supports this relationship between velocity and density.

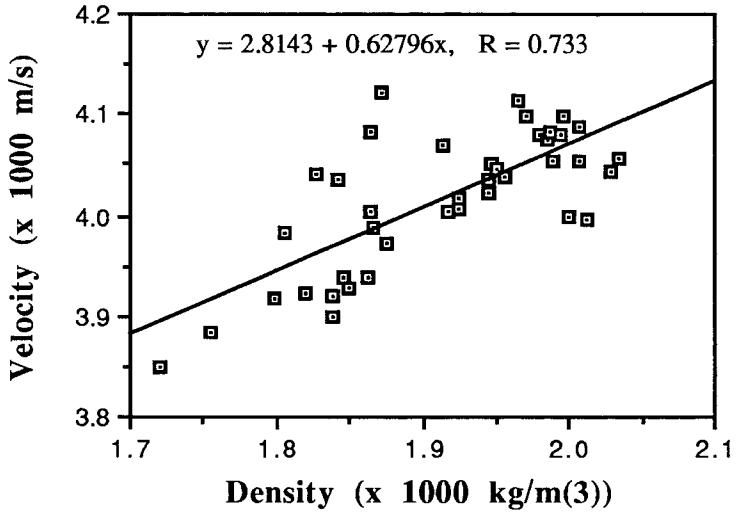

Figure 3.1 *Correlation of Ultrasonic Velocity and Density*

3.1.2 Z and C_{33}

The elastic constant data for the 120 bone cubes (40 sections) calculated from the transmission and water immersion techniques are presented in Table 3A (Appendix A). Meunier's data [20, 25] from two separate experiments are found in Table 3.1 (below)

Table 3.1 *Average Values for the Acoustic Impedance of Bone (Z, 10^{-6} kg/m^{2}s) found by an Ultrasonic Transmission Technique*

Quadrant	Anterior	Posterior	Medial	Lateral
$C_{33avg.a}$	27.1	26.4	28.1	28.0
$C_{33avg.b}$	27.8	26.1	28.7	27.8
$C_{33avg.c}$	31.0	29.1	31.9	31.5

[a] Meunier[20], n=2, ages 25 and 74
[b] Meunier[25], n=20, age range: 48-92
[c] Average value obtained from Table 3A, n=40

so that comparisons can be made. Averaged values from the acoustic transmission experiments for all four variables -- ρ, v, Z, and C_{33} -- of the four quadrants are provided in Table 3.2. Again, the acoustic properties and hence, the elastic constants for the posterior region were significantly lower than the other quadrants (unpaired t-test, $p<0.05$).

Table 3.2 *Averaged Values for Transmission Data from Table 1A (Appendix A), n=40*

Quadrant	Anterior	Posterior	Medial	Lateral
$\rho(g/cm^3)$	1.911	1.855	1.952	1.935
$v(10^3$ m/s)	4.029	3.959	4.042	4.032
$Z(10^{-6}$ kg/m^{2}s)	7.698	7.345	7.891	7.801
C_{33}(GPa)	31.016	29.081	31.897	31.455

It was stated in section 3.1.1 that Meunier's data for the dilational velocities was "lower" when compared quadrant by quadrant to the velocity data, in Table 1A of Appendix A. In turn, the lower acoustic velocities explain why Meunier's [20, 25] values for the acoustic impedance (Z) and the axial elastic stiffness coefficient (C_{33}) for bone are correspondingly lower. More importantly, the values obtained from the transmission techniques are very consistent, comparable to others (Meunier and [22]), and therefore can be considered valid. A major goal of this thesis was to obtain quantitative data from the SAM, and prove the accuracy of the data by comparing values for the acoustic impedance of bone against a known, "proven" technique.

3.2 SAM Scans of Whole Sections

Tables 4A and 5A present the data for 10 of the 30 femoral sections that were scanned, prior to reducing the sections into four quadrants. The 10 proximal sections were chosen to be used in the calculations. The software originally used in calculating the acoustic impedance is explained in section 2.2.4. The values were averaged every 10° in the three

different regions (i.e. the periosteal, middle, and endosteal). Each quadrants properties were determined by superimposing, via software, a pie-shaped wedge to represent that particular quadrant. In Table 4A the acoustic impedance was calculated using all three regions. Table 5A presents only the data acquired from the middle region. Each table also has the corresponding quadrant's acoustic impedance value found with the transmission technique and the reflection coefficient, R(S). The R(S) value is directly related to the Z(S), or Z(Ref) value, and the equations were presented in section 2.2.5. A material with an R(S) value of 1, or a material that totally reflects, would have an infinite impedance. Conversely, a material that does not reflect, would have no impedance. One of the SAM's greatest assets is the acoustic impedance map, which is able to show changes in the material properties of bone on a microscopic scale.

In order to appreciate the relationship between the acoustic impedance mapping obtained with the SAM and the elastic stiffness coefficients obtained on a gross scale from ultrasonic wave propagation, illustrations are presented that show changes in the acoustic properties of cortical bone. It would require a large amount of space, and there would also be a certain amount of redundancy in presenting all 30 sections that were scanned. Therefore two pairs of femurs are being presented (Appendix B, figures 2B (a) and (b)). The femur sections shown in figure 2B (a) were obtained from a 68 year old male (#2265). This scan is an example of two normal sections, where the geometry is slightly altered with the left section being larger than the corresponding right section. The SAM scan is represented with a color distribution scale, where the darkest orange color corresponds to an area of high acoustic impedance and the darkest green color correspondingly represents an area of low impedance. However, the quantity and quality of bone is nearly identical in both sections. Still it can be seen that the posterior section has areas of lower acoustic impedance and endosteal resorption is present throughout the entire medullary canal.

Figure 2B (b), a scan of a pair of femoral sections retrieved from a 78 year old female (#2403), presents a drastic change in bone quality compared to figure 2B (a). It must be

stated again, that the five pairs of femurs used in these experiments did not show great amounts of osteoporosis. Figure 2B (b) is not one of the five sections chosen for the experiments, however, it is one of the femurs that was "rejected". First, differences can be seen between the pair of femoral sections, with the right femur showing less osteoporotic conditions. Observations of extreme differences in acoustic properties between a pair of sections is not an uncommon finding. Second, severe amounts of endosteal resorption are present in the left section, especially in the posterior region, and to a smaller extent in the anterior region.

All of the sections scanned produce an acoustic impedance map which show changes in the material properties over an entire specimen, as evidenced in figures 2B (a) and (b). It is clear from both scans that the distribution in bone acoustic properties is complex and cannot be limited to chosen anatomical quadrants. The acoustic properties vary over much smaller areas than the average quadrant area used in the transmission technique. Also, these images show that the exact location used in the transmission technique is a critical parameter which may effect the elastic constants measurement. A final observation, consistent for all images, is that "low quality bone" (i.e. bone that has a low acoustic impedance) still shows areas of high acoustic properties. This indicates that a decrease in acoustic properties due to remodelling is not a uniform process throughout the cortex, but occurs in certain areas while other areas remain unaffected.

It is well established, and presented earlier (section 1.1.3) that with aging humans lose a substantial amount of bone that was present at 25-30 years of age. It is also obvious that the introduction of a void, or weaker region of bone (as seen in figure 2B), will weaken the entire structure. It is one thing to demonstrate this effect, but another to relate porosity and bone remodelling to the bone structure. The pattern of age-related cortical bone loss involves thinning long bone cortices or cortical thickness loss with a concomitant increase in medullary diameter [10, 37, and 45]. At the same time as bone loss is being added to the periosteal surface, but at a slower rate than during growth [7, 45]. Burr and Martin [1]

have demonstrated that it makes a substantial difference whether the porous region is in the outer, more highly stressed region, or near the medullary canal. By placing "void" spaces near the axis of the medullary canal the "porosity gradient" is actually directed to enhance total bone strength. Finally, Atkinson and Woodhead [44] studied 80 femoral pairs and found tremendous variation in structure, with porosity being well-marked in one region, but minimal in an adjacent region. The SAM scans are able to give orthopaedic investigators another means to study bone remodelling in the femur. However, the SAM's ability to show changes on a microscopic level prior to beginning these experiments was not in doubt. Other investigators have already shown the important "qualitative" information that can be gained from this microscope [20, 21, and 25]. A major hope of this thesis, was not only to provide "qualitative" information, but also accurate "quantitative" information.

Figures 3.2 (next page) plots the data obtained from the transmission experiment (Z-Transm) against the corresponding acoustic impedance values obtained from the SAM (Z-Tot). The correlation factor found from figure 3.4, Z(Tot) vs. Z(Transm), was R=0.633. The extensive bone remodelling accompanying age that is observed for endosteal and periosteal sections has been observed previously. Therefore, it was hoped that the correlation factor would be even higher if the acoustic impedance was calculated from the middle region of the section only, since it is commonly known that bone is remodelling in both the endosteal and periosteal regions (especially in older bone). The correlation of R=0.593 found when Z(Transm) was plotted against Z(Mid) was a slight decrease, but still a fairly good relationship is seen between the transmission technique and the SAM. Again, a statistical difference was found when comparing the posterior section to the other 3 quadrants (unpaired t-test, $p<0.05$).

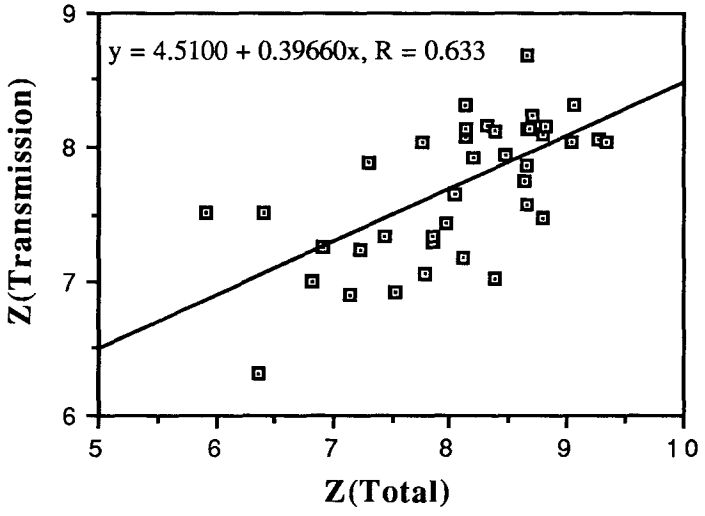

Figure 3.2 *Correlation of Z(Transmission) vs. Z(Total)*

In general, the SAM scans of the whole sections produced important qualitative information and reason to believe that accurate quantitative data can be obtained. The correlation between the Transmission and SAM techniques of 0.639 is good, and several reasons can be cited where improvement is needed. First, the system calculated the acoustic impedance in the three regions - endosteal, middle, and periosteal - and went on to calculate the total acoustic impedance by averaging the three values. Thereby, giving each region equal weight. Second, some amount of error must be accounted for in the assumption of a linear region between glass and plastic (see figure 2.5 (a)). Finally, the transducer (30 MHz) used in the experiments had a small angle and was more suitable for subsurface analysis. As mentioned earlier, at the completion of the scans of the whole sections, a new transducer and a new software program that calculated the acoustic impedance in a different manner were added to the SAM system. It is hoped that future experiments of whole sections of unembedded bone will prove that these changes were useful in attaining better quantitative data.

3.3 SAM Scans of Embedded Cubes

A number of variables were changed in the SAM system before the bone quadrants embedded in PMMA were scanned. Also, the embedding process itself has an impact on the impedance of the SAM, which will be shown in this section. For reference, this process is reviewed in figure 1B (Appendix B). A 50 MHz transducer with 75 um resolution replaced the original 30 MHz transducer and a new software program was added (see section 2.2.4). Therefore two experiments were performed to test the accuracy of the software and the ability to reproduce data.

The first experiment tested the accuracy of the SAM by scanning the embedded bone specimens with two programs that varied the scanning area (ESCAN area $\approx$ 1300 mm^2 and SSCAN area $\approx$ 100 mm^2). Table 3.3 presents the data for both trials of the 5 bone quadrants that were scanned.

Table 3.3 *Correlation of ESCAN vs. SSCAN*

	TRIAL 1		TRIAL 2	
Section	ESCAN	SSCAN	ESCAN	SSCAN
2265R-A	5.43	5.39	5.26	5.25
2265R-P	6.17	6.08	5.86	5.80
2265R-M	4.40	4.30	4.33	4.24
2265R-L	4.69	4.57	4.62	4.49
2279R-A	4.66	4.56	4.59	4.51

The correlation for both trials when plotting ESCAN vs. SSCAN was nearly 1. This is an important finding, because it allows the user to scan different size specimens (i.e. a whole femoral section, and a smaller quadrant from a section) with assurance that the elastic properties will be unchanged. However, it is important to note, that the accuracy of the scan will be greater when a smaller chosen area is used for scanning.

In the second experiment seven embedded cubes were scanned on three different occasions. Table 3.4 presents the acoustic impedance of each trial and the corresponding acoustic impedance that was obtained during the transmission experiments. The correlation

Table 3.4 *Results from SAM experiments to Determine Reproducibilty*

Section	Z(Trial 1)	Z(Trial 2)	Z(Trial 3)	Z(Transm)
2265R-A	7.24	6.68	6.33	7.399
2265R-P	7.28	7.09	5.99	7.199
2265R-L	7.77	6.98	6.42	7.716
2279R-A	6.90	7.18	6.82	7.996
2279R-P	7.29	7.70	6.78	7.692
2279R-M	7.43	8.19	6.63	8.134
2279R-L	8.13	8.37	6.75	8.321

between trial 1, trial 2, and trial 3 vs. the impedance found in transmission was R = 0.752, 0.787, and 0.815 respectively. This proves that the SAM is able to gather accurate acoustic impedance data that can be "related" to the actual values found in transmission. A problem still exists within the software, which causes the variation for the same bone cube from one trial to the next. However, this correlation could have been even stronger if the investigator had known the effects the PMMA embedding process had on the specimens.

The third experiment involved scanning the 39 embedded middle cubes (one cube was destroyed in mechanical testing) and attempting to find a correlation with the transmission technique. Table 6A shows the data obtained for the acoustic properties of bone for both techniques. The first correlation plotted the acoustic impedance of bone found in the transmission technique against the acoustic impedance of the embedded bone found from the SAM. The graph is shown in figure 3.3 (next page), and a poor correlation factor, R = 0.163 was found.

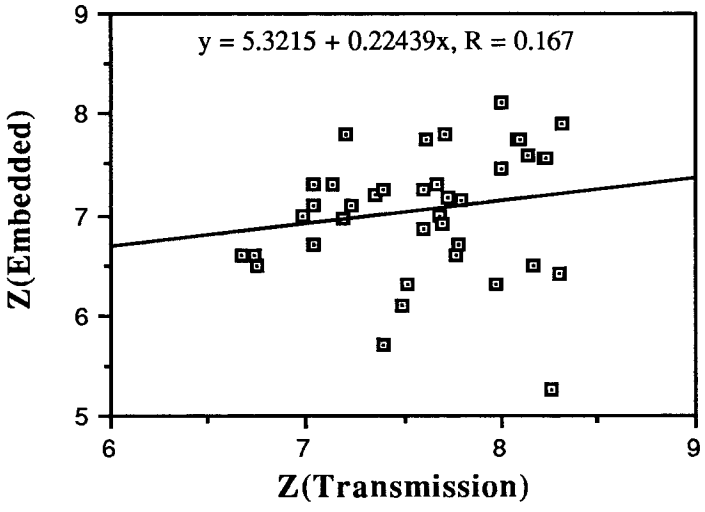

Figure 3.3 *Correlation of Z(Embedded) vs. Z(Transmission), n = 40*

The poor correlation factor found from figure 3.3 can be attributed to the variations in the acoustic impedances of the methacrylate which embedded each cube separately.Table 3.5, along with Table 6A, breaks the embedded cubes into three distinct groups based on the methacrylate's impedance. Also, shown with Table 3.5 is a new correlation between the acoustic impedance of "each" embedded region against that bone's corresponding acoustic impedance found from the traditional Transmission technique.

Table 3.5 *Three Regions of Methacrylate*

Area, Z(Methacrylate)	n	Z(Emb) vs. Z(Transm)
3, 3.1 - 3.2	20	R = 0.853
2, 3.0 - 3.1	6	R = 0.698
1, 2.9 - 3.0	6	R = 0.589

Figure 3.4 presents a new correlation graph, with the 20 embedded cubes (the largest group) plotted against the transmission data. The new correlation of 0.853 shows improvement and a strong relationship is shown between the methacrylate's material properties and the properties of bone. Seven of the embedded cubes were not part of Table 3.5, because the methacrylate's impedance varied over too large a range (>0.15).

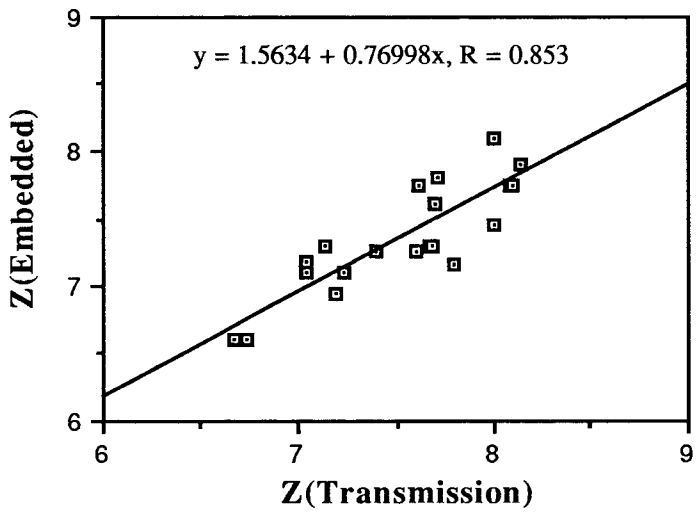

Figure 3.4 *Correlation of Z(Embedded) vs. Z(Transmission), n=20*

A final graph (figure 3.5, next page) is shown to appreciate the relationship that has been witnessed between the properties of the methacrylate and the properties of the embedded bone. This relationship is clear from the separate groups based on their methacrylate's impedance. The embedded bone's impedance in area 3, which is the region with the highest impedance range, is consistently above the impedances of the embedded bone from the other regions. To solidify this relationship more data needs to be acquired. By collecting more data, figure 3.5 will "ideally" have three lines that are parallel to one another (instead of the middle line being skewed).

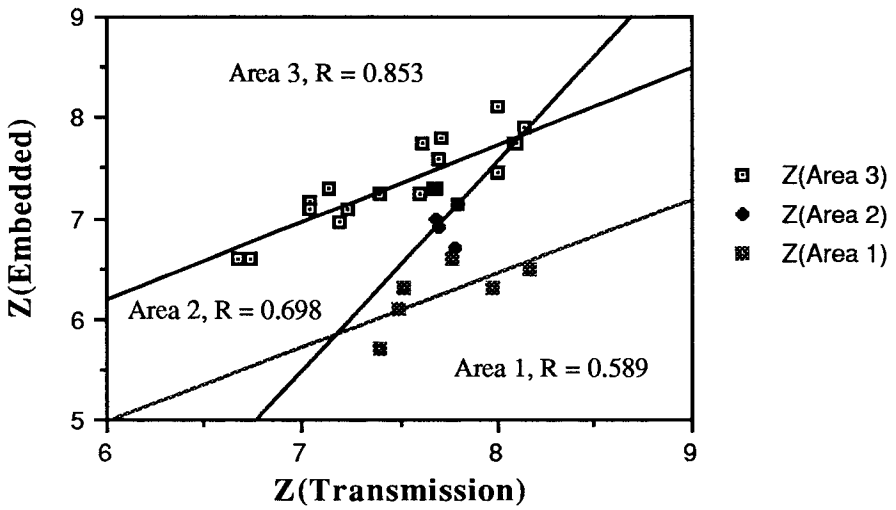

Figure 3.5 *The Three Regions of Methacrylate and their Corresponding Correlations of Z(Embedded) vs. Z(Transmission) - see Table 3.5 and 6A for More Information*

The third experiment was designed to determine if the material properties of embedded bone could be measured relative to the properties of the embedding medium (PMMA). The agreement seen between the acoustic impedance values obtained from the embedded bone against that obtained from the transmission technique gives promise to future SAM scans of embedded materials. However, there are certain limitations to the present SAM which must be stated.

The first reason complete accuracy is still not attainable in the "improved" SAM has been presented in section 3.2. Again, when calibrating the SAM a linear acoustic impedance region is assumed between glass and plastic, where the "true" region is not a straight line. The other two reasons deal with the new software that was added to the system. The user determines (by changing the shape of a rectangle that is superimposed on or within individual regions of a bone section) the region of bone which will be used to find the final "average" impedance value. Therefore, the final average impedance is decided entirely by the rectangle(s) that the user has chosen (not the software). The value

chosen for the average impedance of a bone section almost always needs to be rounded off to a minimum of 0.05, thereby, making the total margin of error +/0 0.15. A second problem with the software exists in choosing the area to be windowed from each histogram obtained from a scan. Without going into a great amount of detail, a narrow window allows the scan to be viewed with more accuracy than a broad window. Through experimentation, it was found that the same parameters must be chosen for each scan. However, by choosing a different sets of parameters for each set of scans one can drastically change the outcome on the data of the embedded cubes from one trial to the next.

Although a strong correlation was shown between the two techniques (SAM vs. Transmission), it cannot be stated that the acoustic impedance data obtained from the embedded bone is equivalent to that of the same bone cube when fresh. At this time, it can only be said that the embedded bone's impedance is "relative" to that of the actual impedance. To improve the SAM equipment and software to narrow the margin of error is possible, but the expense and time that would have to be invested does not make this a worthwhile endeavor.

The power of the SAM qualitatively can't be disputed. A number of general observations can be made concerning the acoustic impedance maps obtained from the scans. The low acoustic impedance of the endosteal and periosteal surfaces were outlined in all of the SAM maps as well as the lower acoustic impedances and more porous bone of the posterior regions. The resolution was also a critical factor to the SAM system. It provided an important link between the bulk values for an entire area and a microscopic picture of the same area. The SAM images provided a measure of material inhomogenity at least three orders of magnitude superior to alternative methods. Each pixel represented an area of 0.01 mm^2 (0.1x0.1 mm) compared to an area of approximately 10 mm^2, as is reasonable for mechanical testing or transmission ultrasonic techniques. The system produced acoustic impedance amplitude profiles that represented real inhomogenities in elastic properties due to the microstructural remodelling of the bone.

3.4 Mechanical Testing

The 40 cubes from the middle sections were to be tested in compression to determine the Modulus of Elasticity (or Young's Modulus), prior to being embedded and scanned (see section 3.3). This data is presented in Table 7A of Appendix A. The 80 proximal and distal cubes were saved for future experiments.

It can clearly be seen from Table 7A that the data is of no value, and this was proved statistically. The Modulus of Elasticity had an extremely large range, 3.691 to 41.305 with an average of 12.7 (GPa), which is much lower when compared to other work [32, 46]. The unsatisfactory data can be attributed to the inhomogeneous nature of the bone material (in porosity, mineralization, and osteonal direction) and more likely due to the specimen size (presumably a larger cross-sectional area - average area of the bone cubes was found to be 34.41 mm^2 with a range from 19.29 to 59.61 - would produce a better averaging of the local inhomogenities). Another important factor with the small surface area, is how hard it is to attain full contact between the bone and the MTS machine.

It was hoped that accurate Mechanical Testing data would give another method to aid in finding and testing the validity of the SAM. Young's Modulus (E) in the longitudinal direction is the inverse of S_{33}, the axial elastic compliance coefficient, and is <u>not</u> equal to C_{33}. However, Young's Modulus may be calculated as a function of orientation with respect to the principal axis of bone symmetry provided the full set of either elastic stiffness or compliance coefficients is available, and in turn, be compared to the C_{33} values obtained from transmission [20]. Other investigators have shown the correlation between the elastic constants determined through transmission and the elastic modulus determined from mechanical testing. Sedlin and Hirsch [34] have established the relationship between the modulus of elasticity of human bone and their ultimate breaking stress. Abendschein and Hyatt [22] even characterized the two moduli (C_{33} and E) in an equation determined by the method of least squares from a graph where the C_{33} from the transmission ultrasonic technique was plotted against the Elastic Modulus from mechanical testing (a correlation of

R=0.9093 was found). Furthermore, they stated that since C_{33} is a function of the velocity of ultrasound in the bone, it follows by a similar correlation that not only the Modulus of Elasticity, but also the breaking strength of bone are directly related to that velocity.

CHAPTER FOUR
CONCLUSIONS

The experiments presented in this thesis have demonstrated the usefulness of the SAM in orthopaedic research. The microscope is able to detect local changes in acoustic impedance and hence, elastic properties at a resolution that is not attainable with other techniques. Other methodologies can directly give elastic constant data (i.e. C_{33}), but this will not provide a description of the inhomogeneous nature of the specimen as observed with the SAM. The thesis verified the SAM's ability to gather qualitative and quantitative data, and showed great promise in retrieving accurate acoustic impedance maps from embedded specimens.

In general, the SAM images of the femoral bone sections were able to show changes that had been documented in the orthopaedic literature. These changes dealt with the remodeling of the endosteal and periosteal regions, and areas of lower acoustic impedance in the posterior region. Quantitatively, from the "fresh" bone scans, a correlation was found between the acoustic impedance values determined with the SAM and the values determined with the traditional transmission technique. The most exciting finding of this thesis was the relationship found between the properties of the methacrylate and the corresponding properties of the bone that it was embedded in. This relationship could eventually mean that every piece of embedded bone could be reexamined for material properties analysis. Presently, more experiments are being performed which will lead to further reinforcing the data presented within this thesis. A proven SAM would have numerous applications in orthopaedic research.

Besides the SAM's ability to analyze the properties from embedded specimens, there are other significant areas of research. The acoustic microscope could be used to produce a better orthopaedic implant. By retrieving a femoral bone section from a pateint who had an implant, the real elastic stiffness data could be implanted into a finite element analysis

model to provide a more accurate model for future implants. The SAM would be the only microscope capable of measuring the mechanical properties of bone from an irregularly shaped area. Two examples would be facet joints in the spine and the insertion sites of ligaments. Finally, a point that has been hammered into the reader throughout the thesis, the SAM would produce real elastic stiffness maps that can be calculated on a microscopic level and not just gross measurements of the bone section over a large area.

APPENDIX A

Table 1A *Ultrasonic Velocity Data*

	DISTAL	VELOCITY MIDDLE	PROXIMAL	AVERAGE VELOCITY
2275L (A)	4.119	4.102	4.142	4.121
2275L (P)	3.957	3.984	3.975	3.972
2275L (M)	4.060	4.076	4.088	4.075
2275L (L)	4.085	4.107	4.103	4.098
2275R (A)	4.070	4.102	4.076	4.083
2275R (P)	3.941	3.932	3.944	3.939
2275R (M)	4.095	4.098	4.071	4.088
2275R (L)	4.074	4.152	4.114	4.113
2279L (A)	3.988	3.98	4.027	3.998
2279L (P)	3.922	4.025	4.02	3.989
2279L (M)	4.013	4.091	4.059	4.054
2279L (L)	4.049	4.058	4.064	4.057
2279R (A)	4.012	3.980	4.000	3.997
2279R (P)	3.996	4.027	3.992	4.005
2279R (M)	4.033	4.079	4.051	4.054
2279R (L)	4.057	4.045	4.025	4.042
2445L (A)	4.008	4.011	4.000	4.006
2445L (P)	4.012	4.038	4.059	4.036
2445L (M)	4.037	4.073	4.095	4.068
2445L (L)	4.046	3.958	4.103	4.036
2445R (A)	4.012	4.000	4.106	4.039
2445R (P)	4.025	3.965	4.060	4.017
2445R (M)	4.085	4.054	4.105	4.081
2445R (L)	4.068	4.029	4.039	4.045
2265L (A)	4.095	4.072	4.124	4.097
2265L (P)	3.981	3.927	4.105	4.004
2265L (M)	4.103	4.049	4.093	4.082
2265L (L)	4.043	3.967	4.142	4.051
2265R (A)	4.018	4.004	4.097	4.040
2265R (P)	3.917	3.947	3.832	3.899
2265R (M)	4.084	4.100	4.052	4.079
2265R (L)	4.013	4.004	4.052	4.023
2286L (A)	3.962	3.958	4.028	3.983
2286L (P)	3.811	3.918	3.919	3.883
2286L (M)	3.971	3.903	3.884	3.919
2286L (L)	3.925	3.871	3.957	3.918
2286R (A)	3.934	3.899	3.947	3.927
2286R (P)	3.872	3.883	3.791	3.849
2286R (M)	3.965	3.948	3.854	3.922
2286R (L)	3.960	3.929	3.928	3.939

UNITS: Velocity, 10^3 meters/second

Table 2A *Density Data*

	DISTAL	DENSITY MIDDLE	PROXIMAL	AVERAGE DENSITY
2275L (A)	1.940	1.870	1.805	1.872
2275L (P)	1.915	1.886	1.825	1.875
2275L (M)	1.948	2.015	1.992	1.985
2275L (L)	1.998	1.942	1.972	1.971
2275R (A)	1.976	1.858	1.762	1.865
2275R (P)	1.914	1.872	1.756	1.847
2275R (M)	2.029	2.016	1.977	2.007
2275R (L)	1.938	1.998	1.959	1.965
2279L (A)	2.042	1.950	2.004	1.999
2279L (P)	1.862	1.837	1.902	1.867
2279L (M)	1.997	2.011	1.955	1.988
2279L (L)	2.038	2.023	2.045	2.035
2279R (A)	2.017	2.009	2.011	2.012
2279R (P)	1.959	1.910	1.882	1.917
2279R (M)	2.019	1.994	2.009	2.007
2279R (L)	2.032	2.057	1.997	2.029
2445L (A)	1.899	1.896	1.981	1.925
2445L (P)	1.966	1.931	1.937	1.945
2445L (M)	1.940	1.840	1.963	1.914
2445L (L)	1.721	1.804	2.005	1.843
2445R (A)	1.933	1.945	1.988	1.955
2445R (P)	1.912	1.917	1.942	1.924
2445R (M)	1.980	1.973	1.988	1.980
2445R (L)	1.972	2.007	1.872	1.950
2265L (A)	1.991	1.886	2.108	1.995
2265L (P)	1.971	1.792	1.830	1.864
2265L (M)	1.962	2.016	1.983	1.987
2265L (L)	1.884	1.948	2.008	1.947
2265R (A)	1.823	1.848	1.814	1.828
2265R (P)	1.865	1.824	1.826	1.838
2265R (M)	2.003	1.974	2.006	1.994
2265R (L)	1.991	1.927	1.913	1.944
2286L (A)	1.769	1.828	1.820	1.806
2286L (P)	1.798	1.703	1.762	1.754
2286L (M)	1.904	1.806	1.808	1.839
2286L (L)	1.803	1.740	1.853	1.799
2286R (A)	1.869	1.844	1.833	1.849
2286R (P)	1.758	1.741	1.662	1.720
2286R (M)	1.863	1.771	1.830	1.821
2286R (L)	1.941	1.793	1.855	1.863

UNITS: Density, 10^3 kilograms/meters^3

Table 3A *Elastic Constant Data*

	AVERAGE DENSITY	AVERAGE VELOCITY	Z	C(33)
2275L (A)	1.872	4.121	7.713	31.786
2275L (P)	1.875	3.972	7.449	29.587
2275L (M)	1.985	4.075	8.088	32.957
2275L (L)	1.971	4.098	8.076	33.100
2275R (A)	1.865	4.083	7.616	31.092
2275R (P)	1.847	3.939	7.277	28.663
2275R (M)	2.007	4.088	8.206	33.546
2275R (L)	1.965	4.113	8.083	33.247
2279L (A)	1.999	3.998	7.991	31.952
2279L (P)	1.867	3.989	7.447	29.708
2279L (M)	1.988	4.054	8.059	32.673
2279L (L)	2.035	4.057	8.257	33.500
2279R (A)	2.012	3.997	8.044	32.154
2279R (P)	1.917	4.005	7.678	30.749
2279R (M)	2.007	4.054	8.138	32.996
2279R (L)	2.029	4.042	8.201	33.149
2445L (A)	1.925	4.006	7.714	30.903
2445L (P)	1.945	4.036	7.849	31.682
2445L (M)	1.914	4.068	7.788	31.685
2445L (L)	1.843	4.036	7.439	30.022
2445R (A)	1.955	4.039	7.898	31.904
2445R (P)	1.924	4.017	7.727	31.036
2445R (M)	1.980	4.081	8.082	32.987
2445R (L)	1.950	4.045	7.890	31.917
2265L (A)	1.995	4.097	8.174	33.487
2265L (P)	1.864	4.004	7.465	29.894
2265L (M)	1.987	4.082	8.110	33.103
2265L (L)	1.947	4.051	7.885	31.941
2265R (A)	1.828	4.040	7.386	29.836
2265R (P)	1.838	3.899	7.167	27.942
2265R (M)	1.994	4.079	8.134	33.177
2265R (L)	1.944	4.023	7.819	31.457
2286L (A)	1.806	3.983	7.191	28.641
2286L (P)	1.754	3.883	6.811	26.447
2286L (M)	1.839	3.919	7.209	28.254
2286L (L)	1.799	3.918	7.047	27.606
2286R (A)	1.849	3.927	7.259	28.504
2286R (P)	1.720	3.849	6.621	25.482
2286R (M)	1.821	3.922	7.144	28.021
2286R (L)	1.863	3.939	7.338	28.906

UNITS: Acoustic Impedance (Z), 10^{-6} kg/m^{2}s and the Elastic Stiffness Coefficient (C_{33}), GPa

Table 4A *Calculations - Total*

	R(S)	Z(Ref)	Z(Trans)
2275L (A)	0.708	8.784	7.476
2275L (P)	0.643	6.909	7.254
2275L (M)	0.704	8.649	8.143
2275L (L)	0.708	8.784	8.091
2275R (A)	0.687	8.099	7.182
2275R (P)	0.668	7.535	6.926
2275R (M)	0.723	9.340	8.048
2275R (L)	0.721	9.265	8.059
2279L (A)	0.688	8.120	8.070
2279L (P)	0.686	8.040	7.646
2279L (M)	0.699	8.473	7.935
2279L (L)	0.716	9.067	8.311
2279R (A)	0.676	7.772	8.044
2279R (P)	0.620	6.405	7.513
2279R (M)	0.689	8.139	8.138
2279R (L)	0.676	7.753	8.038
2445L (A)	0.691	8.200	7.924
2445L (P)	0.704	8.649	7.862
2445L (M)	0.715	9.043	8.038
2445L (L)	0.706	8.694	8.227
2445R (A)	0.694	8.304	8.163
2445R (P)	0.660	7.311	7.885
2445R (M)	0.709	8.807	8.161
2445R (L)	0.704	8.649	7.561
2265L (A)	0.704	8.649	8.693
2265L (P)	0.595	5.910	7.512
2265L (M)	0.697	8.387	8.116
2265L (L)	0.689	8.139	8.317
2265R (A)	0.683	7.962	7.432
2265R (P)	0.639	6.818	6.997
2265R (M)	0.705	8.671	8.128
2265R (L)	0.704	8.626	7.751
2286L (A)	0.665	7.448	7.331
2286L (P)	0.653	7.146	6.905
2286L (M)	0.697	8.387	7.022
2286L (L)	0.679	7.847	7.332
2286R (A)	0.656	7.227	7.235
2286R (P)	0.619	6.378	6.311
2286R (M)	0.677	7.790	7.053
2286R (L)	0.679	7.847	7.286

UNITS: Acoustic Impedance (Z), 10^{-6} kg/m^{2}s

Table 5A *Calculations - Just Middle*

	R(S)	Z(Ref)	Z(Trans)
2275L (A)	0.723	9.312	7.476
2275L (P)	0.654	7.177	7.254
2275L (M)	0.714	8.995	8.143
2275L (L)	0.712	8.924	8.091
2275R (A)	0.711	8.896	7.182
2275R (P)	0.658	7.276	6.926
2275R (M)	0.732	9.682	8.048
2275R (L)	0.728	9.545	8.059
2279L (A)	0.699	8.451	8.070
2279L (P)	0.704	8.649	7.646
2279L (M)	0.721	9.237	7.935
2279L (L)	0.732	9.682	8.311
2279R (A)	0.674	7.712	8.044
2279R (P)	0.647	6.999	7.513
2279R (M)	0.681	7.904	8.138
2279R (L)	0.701	8.536	8.038
2445L (A)	0.708	8.757	7.924
2445L (P)	0.718	9.140	7.862
2445L (M)	0.728	9.522	8.038
2445L (L)	0.721	9.259	8.227
2445R (A)	0.700	8.490	8.163
2445R (P)	0.663	7.392	7.885
2445R (M)	0.709	8.807	8.161
2445R (L)	0.724	9.366	7.561
2265L (A)	0.711	8.896	8.693
2265L (P)	0.594	5.885	7.512
2265L (M)	0.711	8.896	8.116
2265L (L)	0.703	8.602	8.317
2265R (A)	0.700	8.490	7.432
2265R (P)	0.684	7.997	6.997
2265R (M)	0.709	8.805	8.128
2265R (L)	0.719	9.185	7.751
2286L (A)	0.668	7.549	7.331
2286L (P)	0.656	7.211	6.905
2286L (M)	0.705	8.669	7.022
2286L (L)	0.690	8.176	7.332
2286R (A)	0.660	7.311	7.235
2286R (P)	0.609	6.180	6.311
2286R (M)	0.688	8.115	7.053
2286R (L)	0.680	7.881	7.286

UNITS: Acoustic Impedance (Z), 10^{-6} kg/m^{2}s

Table 6A *SAM Data of Embedded Cubes*

	Z(Transm)	Z(EMB)	Z(Meth)	Area
2275L (A)	7.671	7.30	3.07-.15	2/3
2275L (P)	7.514	6.30	2.96-3.04	1/2
2275L (M)	8.213	7.55	3.12-.2	3
2275L (L)	7.976	6.30	2.9-3.0	1
2275R (A)	7.622	7.75	3.15-.2	3
2275R (P)	7.361	7.20	3.23-.26	--
2275R (M)	8.262	5.25	2.8-3.0	1
2275R (L)	8.296	6.40	2.9-3.05	1
2279L (A)	7.761	6.60	2.8-3.07	1
2279L (P)	7.394	5.70	2.9-.96	1
2279L (M)	8.227	7.57	3.07-.25	--
2279L (L)	N/A	N/A	N/A	N/A
2279R (A)	7.996	7.45	3.15-.18	3
2279R (P)	7.692	6.90	3.04-.16	2/3
2279R (M)	8.134	7.60	3.12-.16	3
2279R (L)	8.321	7.90	3.07-.25	--
2445L (A)	7.605	6.85	3.1-.2	3
2445L (P)	7.797	7.15	3.07-.12	2/3
2445L (M)	7 494	6.10	2.88-.95	1
2445L (L)	7.140	7.30	3.1-.2	3
2445R (A)	7.780	6.70	3.06-.12	2/3
2445R (P)	7.601	7.25	3.16-.2	3
2445R (M)	7.999	8.10	3.16-.2	3
2445R (L)	8.086	7.75	3.07-.23	3
2265L (A)	7.680	7.00	2.98-3.13	2
2265L (P)	7.037	7.30	3.15-.2	3
2265L (M)	8.163	6.50	2.93-3.05	1
2265L (L)	7.728	7.18	3.12-.15	3
2265R (A)	7.399	7.25	3.12-.16	3
2265R (P)	7.199	7.80	3.12-.18	3
2265R (M)	8.093	7.75	3.12-.23	3
2265R (L)	7.716	7.80	3.15-.23	3
2286L (A)	7.235	7.10	3.12-.18	3
2286L (P)	6.672	6.60	3.15-.23	3
2286L (M)	7.045	6.70	3.0-.15	--
2286L (L)	6.736	6.60	3.1-.2	3
2286R (A)	7.190	6.95	3.10-.16	3
2286R (P)	6.760	6.50	2.95-3.23	--
2286R (M)	6.992	7.00	2.98-3.16	--
2286R (L)	7.045	7.10	3.13-.25	3

UNITS: Acoustic Impedance (Z), 10^{-6} kg/m^{2}s

Table 7A: *Mechanical Testing Data*

	STRESS	STRAIN	MODULUS
2275L (A)	15.192	0.00182	8.351
2275L (P)	15.873	0.00185	8.580
2275L (M)	12.711	0.00089	14.355
2275L (L)	12.500	0.00205	6.098
2275R (A)	11.364	0.00150	7.586
2275R (P)	6.710	0.00107	6.269
2275R (M)	10.576	0.00120	8.820
2275R (L)	10.293	0.00056	18.453
2279L (A)	20.736	0.00205	10.105
2279L (P)	14.035	0.00174	8.081
2279L (M)	16.136	0.00228	7.085
2279L (L)	N/A	N/A	N/A
2279R (A)	20.284	0.00183	11.085
2279R (P)	11.425	0.00093	12.351
2279R (M)	14.551	0.00111	13.058
2279R (L)	17.945	0.00217	8.288
2445L (A)	8.110	0.00167	4.866
2445L (P)	8.280	0.00183	4.532
2445L (M)	15.486	0.00171	9.031
2445L (L)	17.483	0.00112	15.549
2445R (A)	12.255	0.00048	25.312
2445R (P)	7.570	0.00075	10.028
2445R (M)	13.219	0.00084	15.709
2445R (L)	18.165	0.00066	27.321
2265L (A)	20.502	0.00088	23.329
2265L (P)	10.499	0.00116	9.037
2265L (M)	14.625	0.00042	35.003
2265L (L)	13.373	0.00032	41.305
2265R (A)	14.540	0.00135	10.760
2265R (P)	8.409	0.00192	4.386
2265R (M)	11.186	0.00086	12.975
2265R (L)	11.236	0.00116	9.663
2286L (A)	14.782	0.00122	12.134
2286L (P)	10.753	0.00072	15.037
2286L (M)	10.119	0.00190	5.325
2286L (L)	10.501	0.00209	5.025
2286R (A)	11.354	0.00055	20.644
2286R (P)	6.988	0.00036	19.267
2286R (M)	8.637	0.00127	6.779
2286R (L)	7.644	0.00207	3.691

UNITS: Elastic Modulus (E), GPa

APPENDIX B

Figure 1B *Schedule for Embedding Calcified Bone Samples in Hard PMMA Solution*

Embedding for small calified bone: Approximately 10x5x5 mm
Dehydrate over 4 days.
Infiltrate in each methyl methacrylate solution for 3 days.

DAY 1	Overnight	40% Ethanol (24 Hours)
DAY 2	9:00 to 5:00	40% Ethanol (8 Hours)
	5:00 to Next Morning	70% Ethanol (16 Hours)
DAY 3	9:00 to 5:00	80% Ethanol (8 Hours)
	5:00 to Next Morning	80% Ethanol (16 Hours)
DAY 4	9:00 to 5:00	95% Ethanol (8 Hours)
	5:00 to Next Morning	95% Ethanol (16 Hours)
DAY 5	9:00 to 5:00	100% Ethanol (8 Hours)
	5:00 to Next Morning	100% Ethanol (16 Hours)
DAY 6	9:00 to 1:00	Hemo-De (4 Hours)
	1:00 to 5:00	Hemo-De (4 Hours)
	5:00	Hard Methyl Methacrylate I (3 to 7 Days)
DAY 9	For at least 3 days	Hard Methyl Methacrylate II (3 to 7 Days)
DAY 12	For at least 3 days	Hard Methyl Methacrylate III (3 to 7 Days)
DAY 15	Place bottle in waterbath	Hard Methyl Methacrylate III (3 to 7 Days)

DAY 16 When the solution has polymerized, the bottle is labelled. Add more methyl methacrylate solution, and place the bottle in the waterbath.

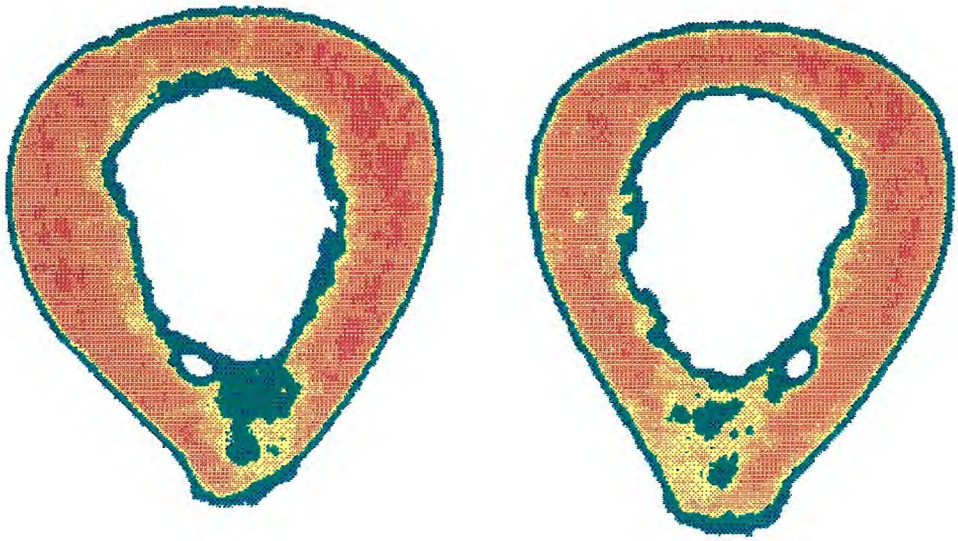

Figure 2B (a) Pair of femoral sections (#2265) scanned with the SAM

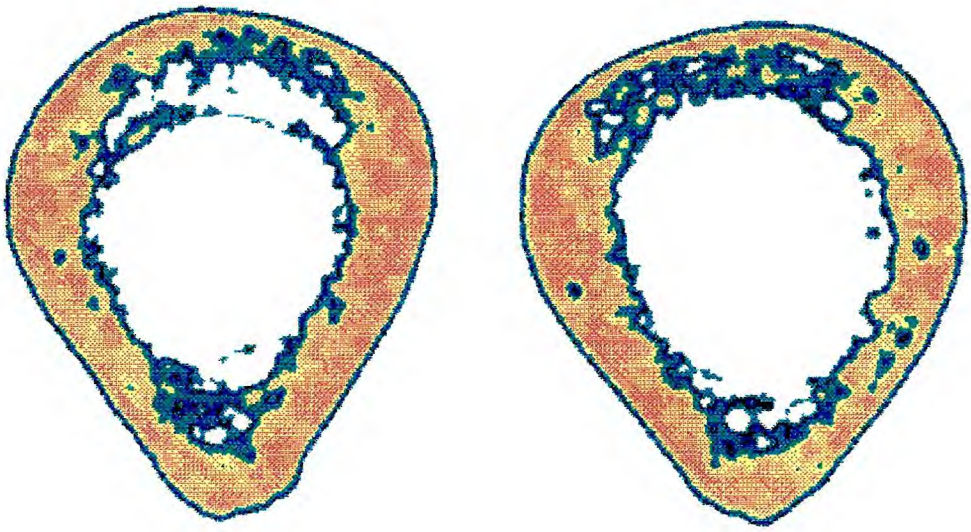

Figure 2B (b) Pair of femoral sections (#2403) scanned with the SAM

REFERENCES

1. Martin, R.B., and D.B. Burr. Structure, Function, and Adaption of Compact Bone Raven Press, New York (1989).

2. Treharne, R.W. "Review of Wolff's Law and its Proposed Means of Operation." *Orthopaedic Review* 10 (1981): 35-47.

3. Lanyon, L.E. Mechanical Function and Bone Remodelling In: Summer-Smith G(ed) Bone in Clinical Orthopaedics. W.B. Saunders, Philadelphia (1982): 273.

4. Carter, D.R. "Mechanical Loading Histories and Cortical Bone Remodelling." *Calcified Tissue International* 36 (1984): S31-S36.

5. Cooper, K.H. "The Basics of Bone." *Health* (1989): 81-82.

6. Garn, S.M. The Earlier Gain and the Later Loss of Cortical Bone Charles C. Thomas, Springfield, Ill. (1970).

7. Smith, R.W., and R.W. Walker. "Femoral Expansion in Aging Women: Implications for Osteoporosis and Fractures." *Science* 145 (1964): 156-157.

8. Jaworski, Z.F.G., M. Liskova-Kiar, and H.K. Uhthoff. Regional Disuse Osteoporosis and Factors Influencing its Reversal In:H.K. Uhthoff and E. Stahl (eds) Current Concepts of Internal Fixation of Fractures. Springer-Verlag, New York. (1980): 17-26.

9. Atkinson, P.J. "Quantitative Analysis in Cortical Bone." *Nature* 201 (1964): 373-375.

10. Jowsey, J. "Age Changes in Human Bone." *Clinical Orthopaedics and Related Research* 17 (1960): 210-217.

11. Kessler, L.W. "Acoustic Microscopy." In "Metals Handbook", Vol. 17, 9th Edition: Nondestructive Evaluation and Quality Control, ASM International, Materials Park, Ohio (1989): 465-482.

12. Lemons, R.A., and C.F. Quate. "Acoustic Microscope Scanning Version." *Appl. Phys. Lett.* 24 (1974): 163.

13. Jipson, V., and C.F. Quate. "Acoustic Microscopy at Optical Wavelengths." *Appl. Phys. Lett.* 32 (1978): 789.

14. Briggs, A. An Introduction to Scanning Acoustic Microscopy New York, Oxford University Press (1985).

15. Nonaillard, B., J.M. Rouvaen, and N.E. Imouloudene "Nondestructive Evaluation of Composite Materials Using Acoustic Microscopy." In Acoustical Imaging, Schimizu, H., N. Chubachi, and J. Kushibiki(eds), New York: Planum Press (1989): 111-119.

16. Breiter-Hahn, J., J. Litniewski, K. Hillmann, A. Krapohl, and L. Zylberg. "What can Scanning Acoustic Microscopy Tell about Animal Cells and Tissues?". In Acoustical Imaging, Schimizu, H., N. Chubachi, and J. Kushibiki(eds), New York: Planum Press (1989): 27-38.

17. Hildebrand, J.A., D. Rugar, R.N. Johnston, and C.F. Quate. "Acoustic Microscopy of Living Cells." *Proceeding of the National Academy of Sciences, USA* 78, 3 (1981): 1656-1660.

18. Kasahara, S., K. Yoshida, J. Kushibiki, and N.L. Chubachi. "Application of Acoustic Microscopy in Dental Research." In Acoustical Imaging, Schimizu, H., N Chubachi, and J. Kushibiki (eds), New York: Planum Press (1989): 153-158.

19. Briggs, G.A.D., C.M.W. Daft, A.F. Fagan, T.A. Field, C.W. Lawrence, M. Montoto, S.D. Peck, A. Rodriguez, and C.B. Scruby. "Acoustic Microscopy of Old and New Materials." In Acoustical Imaging, Schimizu, H., N. Chubachi, and J. Kushibiki(eds), New York: Planum Press (1989): 1-16.

20. Meunier, A., J.L. Katz, P. Christel, and L. Sedel. "A Reflection Scanning Acoustic Microscope for Bone and Bovine Biomaterials Interface Studies." *Journal of Orthopaedic Research* 6 (1988): 770-775.

21. Zimmerman, M.C., A. Meunier, J.L. Katz, and P. Christel. "The Evaluation of Cortical Bone Remodelling with a New Ultrasonic Technique." *IEEE Transactions on Biomedical Engineering* 37, 5 (1990): 433-441.

22. Abendschein, W., and G.W. Hyatt. "Ultrasonics and Selected Physical Properties of Bone." *Clinical Orthopaedics and Related Research* 69 (1970): 294-301.

23. Katz, J.L., H.S. Yoon, S. Lipson, R. Maharidge, A. Meunier, and P. Christel. "The Effects of Remodelling in the Elastic Properties of Bone." *Calcified Tissue International* 36 (1984): S31-S36.

24. Lang, S.B. "Ultrasonic Method for Measuring Elastic Coefficients of Bone and Results on Fresh and Dried Bovine Bone." *IEEE Transactions on Biomedical Engineering* 17, 2 (1970): 101-105.

25. Meunier, A., O. Riot, P. Christel, and J.L.Katz. "Characterization of Local Anisotropic Elastic Properties of Femoral and Tibial Diaphysis Using Acoustic Transmission Measurements and Acoustic Microscopy." In Interfaces in Medicine and Mechanics II, K.R. Williams, A. Toni, J. Middleton, and G. Pallotti (eds), Elsevier Applied Science, London (1991): 454-463.

26. Yoon, H.S., J.L. Katz. "Ultrasonic Wave Propagation in Human Cortical Bone -- II. Measurements of Elastic Properties and Microhardness." *Journal of Biomechanics* 9 (1976): 459-464.

27. Ashman, R.B., S.C. Cowin, and W.C. Van Buskirk. "A Continuous Wave Technique for the Measurement of the Elastic Properties of Cortical Bone." *Journal of Biomechanics* 17 (1984): 349-361.

28. Yoon, H.S., and J.L. Katz. "Ultrasonic Wave Propagation in Human Cortical Bone -- I. Theoretical Considerations for Hexagonal Symmetry." *Journal of Biomechanics* 9 (1976): 407-412.

29. Meunier, A., H.S. Yoon, J.L. Katz, P. Christel P, and F. Vosburgh. "Ultrasonic Characterization of some Pathological Human Femora." Presented at *IEEE Ultrasonic Symposium*, San Diego, CA (1982): 713-717.

30. Yoon, H.S., and J.L. Katz JL. "Ultrasonic Wave Propagation in Human Cortical Bone. I. Theoretical Considerations for Hexagonal Symmetry." *Journal of Biomechanics* 9 (1976): 407-412.

31. Cowin S.C. Bone Mechanics Florida: CRC Press (1989): 99-127, 253-277.

32. Van Buskirk, W.C.. and R.B. Ashman. "The Elastic Modulus of Bone." In 1981 Biomechanics Symposium, W.C. Van Buskirk and SL-Y Wood (eds), New York: ASME (1981): 131-143.

33. Roark, R.J. Formulas for Stress and Strain, ed. 4, New York, McGraw-Hill Book Co. (1965).

34. Sedlin, E.D., and C. Hirsch. "Factors Affecting the Determination of Physical Properties of Femoral Cortical Bone." 7 *Acta. Orthop Scand* (1966): 29.

35. Mather, B.S. "Correlations Between Strength and Other Properties of Long Bones." *Journal of Trauma* 7 (1967): 633.

36. Generazio, E.R., D.J. Roth, and G.Y. Backlini. "Imaging Subtle Microstructural Variations in Ceramics with Precision Ultrasonic Velocity and Attenuation Measurements." In *NASA Technical Memorandum 100129*, Cleveland, Ohio (1987): 1-6.

37. Consensus Development Panel. "Total Hip Joint Replacement" NIH - consensus paper, JAMA 248 (1982): 1817-1821.

38. Blacker, G., and J. Charnley. "Changes in the Upper Femur After Low Friction Arthroplasty." *Clinical Orthopaedics and Related Research* 137 (1978): 15-24.

39. Carter, D.R., R. Vasu, D.M. Spangler, and R.T Riceland. "The Mechanical and Biological Response of Cortical Bone to In Vivo Strain Histories." In: Cowin SC (ed) Mechanical Properties of Bone, American Society of Mechanical Engineering, New York (1981): 81.

40. Tonino, A.J., C.L. Davidson, P.J. Klopper, and L.A. Lindau LA. "Protection from Stress in Bone and its Effects." *Journal of Bone and Joint Surgery* 58(1) (1976): 107-113.

41. Goodship, A.E., L.E. Lanyon, and H. MacFie H. "Functional Adaption of Bone to Increased Stress." *Journal of Bone and Joint Surgery* 61(4) (1979): 539-546.

42. Berndt, H: Personal Communication.

43. Meunier, A: Personal Communication.

44. Atkinson, A.J., and C. Woodhead. "The Development of Osteoporosis." *Clinical Orthopaedics and Related Research* 90 (1973): 217-228.

45. Parfitt, A.M. "Age-Related Structural Changes in Trabecular and Cortical Bone: Cellular Mechanisms and Biomechanical Consequences." *Calcified Tissue International* 36 (1984): S123-S128.

46. Reilly, D.T., and A.H. Burstein. "The Elastic and Ultimate Properties of Compact Bone Tissue." *Journal of Biomechanics* (1975): 393-405.